ADVANCED MATERIALS
www.advmat.de

Materials with Electroprogrammable Stiffness

David J. Levine, Kevin T. Turner, and James H. Pikul**

Stiffness is a mechanical property of vital importance to any material system and is typically considered a static quantity. Recent work, however, has shown that novel materials with programmable stiffness can enhance the performance and simplify the design of engineered systems, such as morphing wings, robotic grippers, and wearable exoskeletons. For many of these applications, the ability to program stiffness with electrical activation is advantageous because of the natural compatibility with electrical sensing, control, and power networks ubiquitous in autonomous machines and robots. The numerous applications for materials with electrically driven stiffness modulation has driven a rapid increase in the number of publications in this field. Here, a comprehensive review of the available materials that realize electroprogrammable stiffness is provided, showing that all current approaches can be categorized as using electrostatics or electrically activated phase changes, and summarizing the advantages, limitations, and applications of these materials. Finally, a perspective identifies state-of-the-art trends and an outlook of future opportunities for the development and use of materials with electroprogrammable stiffness.

1. Introduction

Stiffness is a fundamental material property that often defines the mechanical interaction between a material and the world. Materials designed to achieve a target stiffness are, therefore, ubiquitous in engineered systems. Compliant systems made from soft materials (1 to 10^5 kPa)[1] conform to their local environment and redistribute loads, with notable examples including flexible implants for biomedicine,[1–3] elastomeric gaskets for high-performance seals,[4] and compressible soles to increase the comfort and responsiveness of shoes.[5] Materials with high stiffness (10^5 to 10^8 kPa)[1] are advantageous for supporting large loads with minimal deflection. Notable examples include airframes, fatigue-resistant tools, and machine frames that transmit large forces.[6] In the majority of engineered systems, stiffness is designed to be a static quantity and engineers often optimize a single design to accommodate trade-offs between soft and stiff components.[7] However, an increasing number of applications would benefit from materials with a stiffness that can be actively changed, or programmed.

Biological systems, for example, routinely modulate their stiffness to achieve specific functions. **Figure 1** shows examples of biological systems that use stiffening for muscle-driven locomotion and object manipulation, or softening for shape modification.[8–10] An elephant trunk, for example, can quickly stiffen to lift and support heavy objects, but also rapidly soften to manipulate small, delicate items without damage.[11] Similarly, an octopus can selectively stiffen different sections of their tentacles to grab objects, and soften to negotiate through confined spaces.[12] Most vertebrates tune their stiffness by controlling the bonding of actin and myosin proteins contained in striated muscle tissue.[13,14] Soft-bodied invertebrates, such as, the sea cucumber, link and unlink collagenous fibers embedded within dermal layers to quickly stiffen when attacked.[15] Aerial insects, such as flies, alter the stiffness of intrinsic wing muscles to steer and direct power from primary flight muscles.[16] The ability of biological systems to dynamically modulate their stiffness allows for on-demand responses to environmental changes and elegant functionality that would be unachievable with a constant stiffness.

In a similar manner, many engineered technologies benefit from materials whose stiffness can be programmed. These materials have been rapidly gaining attention due to their applications in robotics, aerodynamics, haptics, and biomedical devices. The materials in soft robotic actuators and wearable exoskeletons, for example, increase their mechanical stiffness to enable the autonomous formation of complex shapes,[7] or to match the impedance of a patient in need of rehabilitation.[1,17,18] Additionally, soft materials in prosthetic devices have been programmed to stiffen and lock-in specific shapes for low-energy grasping of objects.[19] These materials with programmable stiffness enable multifunctional machines with simple designs, whose properties can be adjusted to accomplish varying tasks in real time. While several applications show the promise of this approach, new materials with large changes in programmable stiffness are required to enable emerging applications with more extreme performance, design, and integration requirements, such as haptics[20,21] and artificial morphing wings for increased aerodynamic performance.[22,23,42]

Several stimuli can trigger a programmable and reversible stiffness change in a material system. Some examples include, pressurized pneumatic[3,5,17,18,24] or hydraulic[25] fluids, vacuum-induced jamming of granular,[26] or laminar materials,[27] motor-driven tendons,[28] changes in temperature,[29,30] optical excitation,[31] or the presence of an external magnetic field.[32,33] While all of these inputs are advantageous in specific scenarios, they each have notable disadvantages. Some stimuli require

D. J. Levine, Prof. K. T. Turner, Prof. J. H. Pikul
Department of Mechanical Engineering & Applied Mechanics
220 S. 33rd St., Philadelphia, PA 19104, USA
E-mail: kturner@seas.upenn.edu; pikul@seas.upenn.edu
The ORCID identification number(s) for the author(s) of this article can be found under https://doi.org/10.1002/adma.202007952.

DOI: 10.1002/adma.202007952

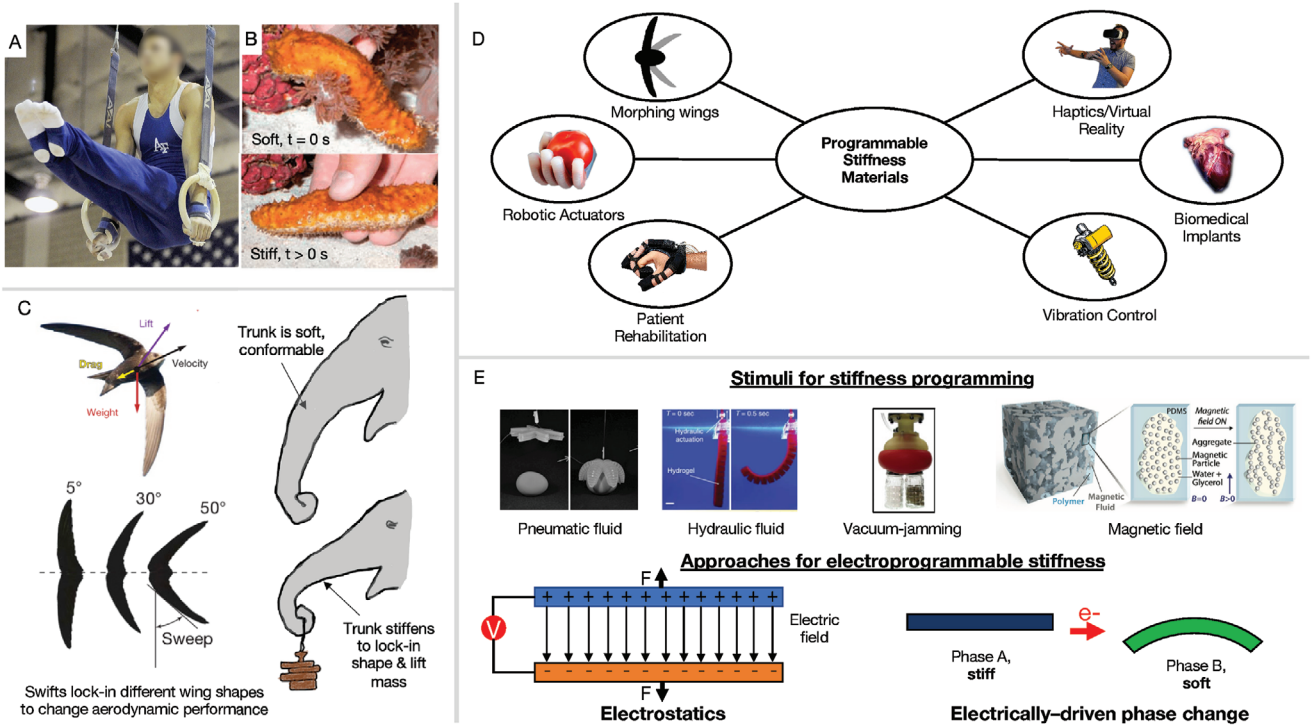

Figure 1. Programmable stiffness in biology and engineering. Biological systems are capable of significant stiffness changes. A) Humans routinely increase the stiffness of their muscles to perform tasks. B) Sea cucumbers increase the stiffness of their dermal layer as a means of protection. C) Swifts change the stiffness of their wings to dynamically alter aerial efficiency, while elephants can use their trunk in its soft state to conform to delicate objects and stiffen it to carry large loads. D) Programmable stiffness materials are increasingly used in engineering fields, including robotics, biomedicine, air vehicles, and virtual reality. E) Many stimuli have been used to program stiffness changes in material systems, but materials with electroprogrammable stiffness are easily integrated and enhanced with electronics, and are either driven by electrostatics or an electrically driven phase transitions. B) Reproduced with permission.[15] Copyright 2008, AAAS. C) Swifts in flight image: Reproduced with permission.[10] Copyright 2007, Springer Nature. Elephant drawings: Reproduced with permission.[11] Copyright 1991, ASME. D) Image for "Robotic Actuators": Reproduced with permission.[43] Copyright 2016, AAAS. Image for "Patient Rehabilitation": Reproduced with permission.[17] Copyright 2015, Elsevier. E) Images for "Stimuli for stiffness programming": Images for "Pneumatic Fluid": Reproduced with permission.[44] Copyright 2011, Wiley-VCH. Images for "Hydraulic Fluid": Reproduced under the terms of the CC-BY Creative Commons Attribution 4.0 International license (https://creativecommons.org/licenses/by/4.0).[25] Copyright 2017, The Authors, published by Springer Nature. Images for "Vacuum Jamming": Reproduced with permission.[45] Copyright 2012, IEEE. Images for "Magnetic Field": Reproduced with permission.[32] Copyright 2019 Wiley-VCH. Image in (A) and images for "Haptics/Virtual Reality" and "Vibration Control" in (D) are from Pixabay (CC0).

bulky equipment that add considerable design complexity, weight, and cost to engineered systems, while others lead to slow, non-uniform material responses.[32] Electrically activated stimuli are advantageous because of their compatibility with electrical sensing, control, and power networks ubiquitous in autonomous machines and robots. Additionally, electrical signals can be accurately and rapidly transmitted within a material for spatial stiffness control.[34] The numerous applications that benefit from electrically driven stiffness modulation and the rapid increase in material systems that realize electroprogrammable stiffness requires a comprehensive review to organize the results and identify future opportunities. Prior review articles have concentrated on general methods for stiffness change in robotic technologies,[1,19,35–37] stiffness change for switchable adhesion,[38] stiffness modulation using multifunctional liquid-metal composites[39] and dielectric elastomer actuators,[40,41] but none of these works provide a comprehensive picture of the materials that enable electroprogrammable stiffness.

Herein, we review materials with electroprogrammable stiffness. Materials with electroprogrammable stiffness are defined as materials that change their mechanical stiffness in response to electrical stimuli. We found that current examples of such materials utilize either electrostatics or phase-changes to modulate stiffness, and these defining physics divide the review into two primary sections. Each section is organized by material systems that exploit electrostatics or phase-changes. For each system, we summarize the governing physics and discuss the advantages and limitations of the different materials that exploit these physics. We then explain how materials selection and design play a critical role in device performance and compare state-of-the-art examples. Finally, we detail challenges in the field and provide an outlook for future opportunities in materials with electroprogrammable stiffness.

2. Overview

Figure 2 shows a comprehensive summary of material stiffness changes for state-of-the-art materials with electroprogrammable stiffness, which is organized by lowest applied

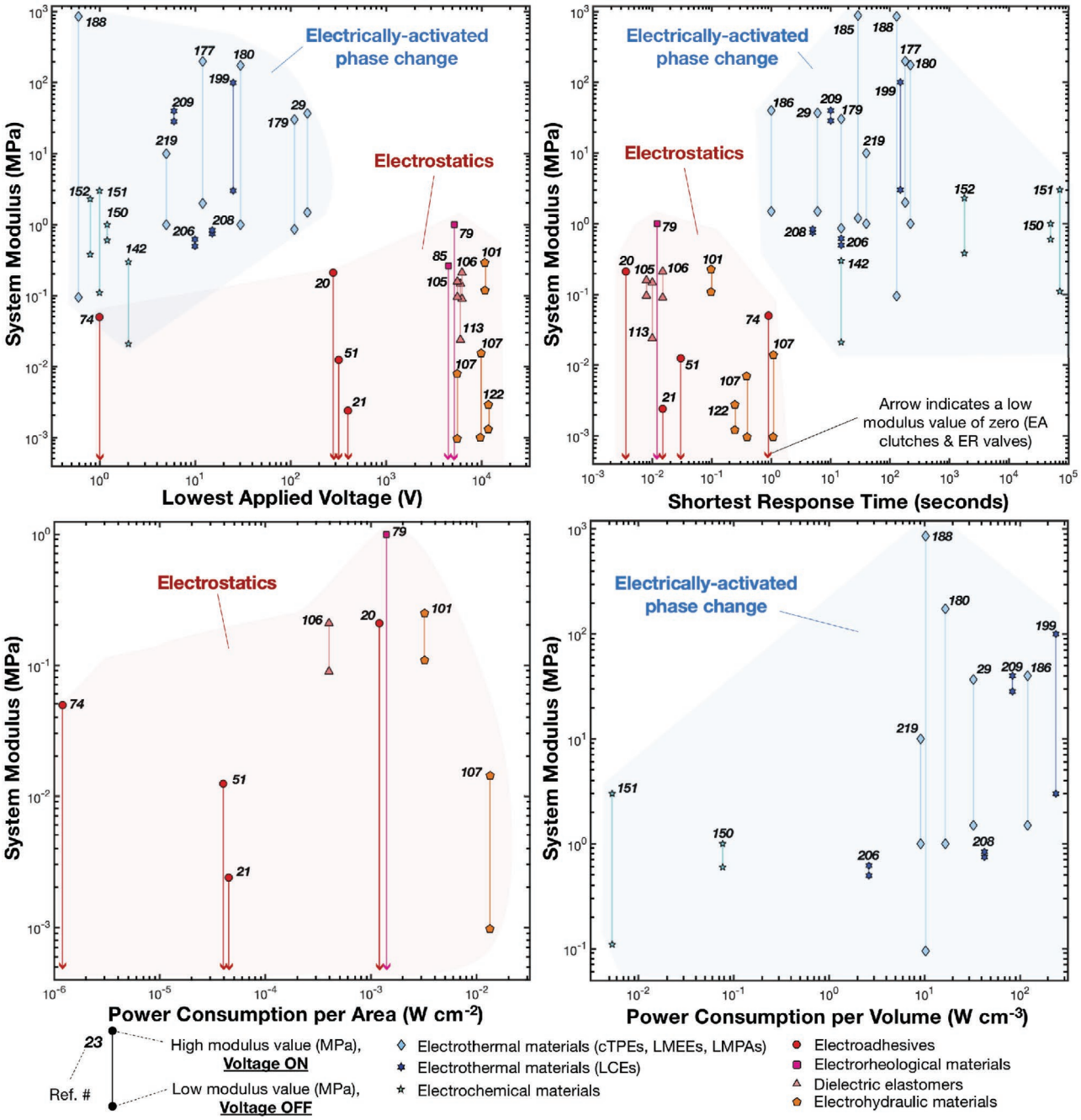

Figure 2. A quantitative summary of state-of-the-art materials with electroprogrammable stiffness. Individual data points show the activated and de-activated moduli of a given electroprogrammable material system as a function of their lowest applied voltage (top left), shortest response time (top right), normalized power consumption per area for electrostatic materials (bottom left), and normalized power consumption per volume for electrically activated phase-change materials (bottom right). A material's lowest applied voltage is the smallest voltage value that can be used to trigger the maximum degree of stiffness change, and the shortest response time is the time required for that change to occur. Normalized power consumption is the amount of power required to generate the maximum stiffness change within the activation time.

voltage and shortest response time in two charts. From these charts, it is evident that materials with electroprogrammable stiffness governed by electrostatics, including electroadhesives, electrorheological materials, dielectric elastomers, and electrohydraulics, can be activated and de-activated quickly (in milliseconds), but require high activation voltages (>300 V) and $<10^{-2}$ W cm^{-2} power to trigger a meaningful stiffness change, which we define as an increase or decrease in system modulus greater than 50 kPa. In contrast, materials with electroprogrammable stiffness governed by electrically driven phase transitions, including electrochemical and electrothermal materials, require smaller activation voltages (<100 V),

consume <100 W cm^{-3} power, and have longer activation and de-activation times than electrostatic materials (on the order of seconds to minutes). These general characteristics are determined by the underlying physics of the materials: electrically driven phase transitions require the diffusion of heat or ions while electrostatic methods can be rapidly triggered by the introduction of an electric field. Furthermore, small voltages are required to induce Joule heating or electrically driven redox reactions, while electrostatic approaches rely on large input voltages to generate attractive forces or particle alignment within a material or fluid. From Figure 2, it is also clear that the overall degree of stiffness change is generally larger for electroprogrammable materials governed by phase transitions compared to that of materials based on electrostatics. However, their increased power consumption increases the size and weight of required power supplies. Electrostatic materials, in contrast, have high operating voltages which present challenges in the design of electronic boards for untethered applications, as voltage amplifiers are required that add additional mass and cost. Nevertheless, the smaller activation/de-activation times for electrostatic materials increases their compatibility with off-the-shelf electronics systems, and make them increasingly attractive for applications that require real-time high-frequency stiffness programming, such as autonomous rehabilitation devices and untethered soft robots.

3. Electroprogrammable Stiffness via Electrostatics

3.1. Electroadhesives

When an electric potential is applied between two conductive surfaces, an electric field is generated between them and opposite charges on the respective electrodes are attracted to each other via electrostatic forces, resulting in electroadhesion of the surfaces.[46] Materials that use electroadhesion for stiffness modulation are often comprised of two (or more) conductive, overlapping electrodes separated by an insulating dielectric material. When no voltage is applied between the electrodes, the layers can freely slide past one another and the stiffness is dictated by the stiffness of the surrounding medium. When a voltage (typically ranging from 0.1 to 6 kV)[47] is applied, electrostatic forces from aligned dipoles in the dielectric pull the overlapping sections of the electrodes together. The resulting normal force between electrodes allows frictional forces at the contacting interface to resist in-plane sliding and increase the in-plane stiffness. Stiffness changes due to electroadhesion occur in milliseconds and the response time depends on the applied voltage, electrode resistance, and system capacitance.[47]

Figure 3A shows two types of electrostatic attraction between materials. Coulombic attraction occurs in insulating dielectrics where charges are immobile and Johnsen–Rahbek attraction occurs in dielectrics with higher conductivity where charges can move through the separating layer. Below, we review models that describe the interaction forces, and discuss the situations where each are valid. Finally, we describe how the different interaction forces affect the performance and materials selection of electroadhesives.

3.1.1. Coulombic Electroadhesion

For two flat parallel surfaces, the coulomb force generated by an applied electric field can be expressed as

$$F_c = \frac{A}{2}\varepsilon_o\left(\frac{k_d V}{d}\right)^2 \quad (1)$$

where A is the contact area between the electrodes, V is the applied voltage, d is the thickness of the dielectric layer, ε_o is the permittivity of free space and k_d is the relative permittivity of the dielectric layer.[48] In this simple model, the attractive force is proportional to k_d^2, which arises due to the presence of a gap (of either air or vacuum) of infinitesimal size at the bond interface because of imperfect contact between the layers. Here, the dielectric and gap act as capacitors in series and result in a different formulation than coulombic attraction between the plates of a perfect parallel plate capacitor, which predicts that the attractive coulomb force is proportional to k_d when there are no gaps at the bond interface. While many studies use the simple parallel plate capacitor model to describe Coulomb electroadhesion, Persson et al. showed that accounting for the gap, and net surface roughness of dielectric and electrode materials, more accurately predicted the output force.[49] The small interfacial air gap effectively concentrates the electric field, increasing the overall electrostatic attraction between the plates.

3.1.2. Johnsen–Rahbek Electroadhesion

Materials that use electroadhesion for stiffness modulation often assume the dielectric layers to be fully insulating, but this is not always an accurate representation.[50] When charge carriers can move through the dielectric layer, electroadhesion occurs via the Johnsen–Rahbek (J–R) effect.[46] In this case, current flows through the dielectric (e.g., a polyelectrolyte or a semiconducting material) and charges migrate to the surfaces of the dielectric film. The electric field is generated across a nanometer-scale interfacial gap between the edges of the touching dielectric layers, or between the edge of the dielectric layer and the opposite electrode. The attractive force due to the J–R effect can be calculated as

$$F_{JR} = \frac{A_{real}}{2}\varepsilon_o\left(\frac{k_g V_{eff}}{g}\right)^2 \quad (2)$$

where A_{real} is the real contact area between the nanoscale asperities on the surfaces, g is the size of the interfacial gap, k_g is the relative permittivity of the interfacial gap and V_{eff} is the effective applied voltage.[48] V_{eff} is a function of the equivalent resistances of the bulk dielectric volume and the contact interface, which effectively acts as a voltage divider. For any electroadhesive interface, attractive forces due to both coulomb and J–R effects are present simultaneously between surfaces. However, J–R forces dominate when the bulk resistivity of the dielectric material is less than 10^{10} Ω cm, and coulombic forces

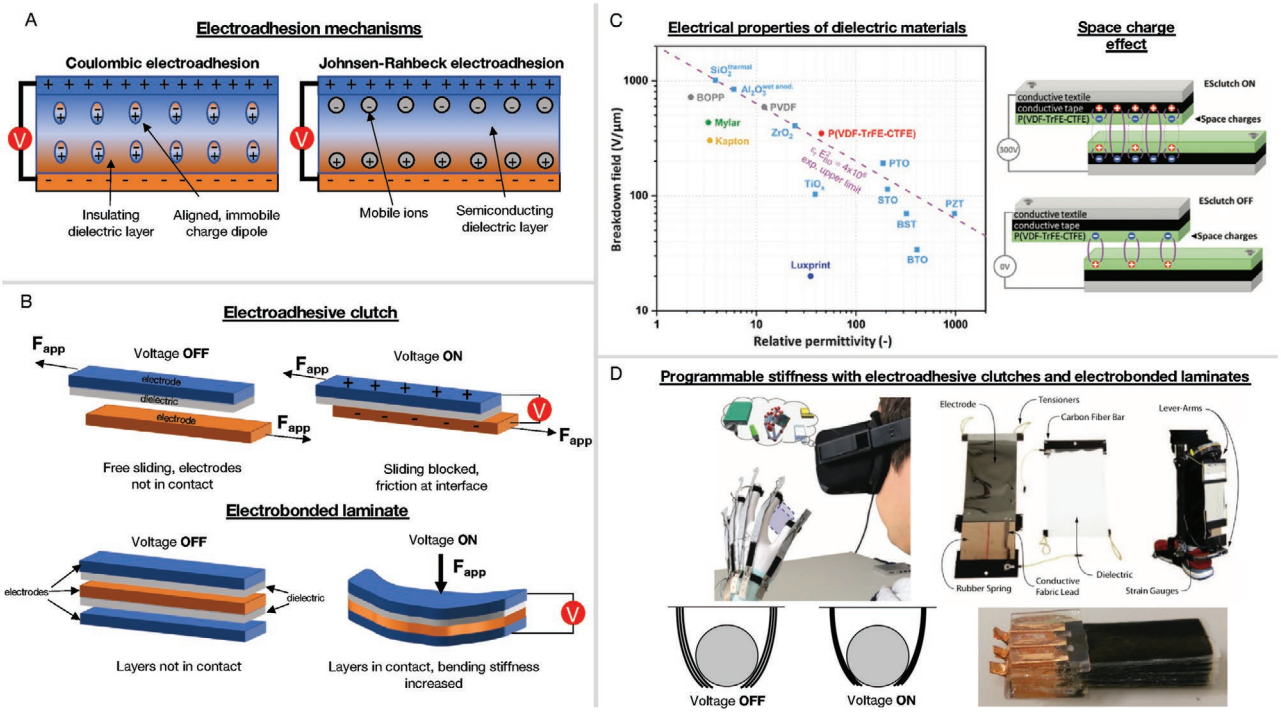

Figure 3. Electroadhesives (EAs). A) Two types of electroadhesion: Coulombic and Johnsen–Rahbek (J–R). For coulombic electroadhesives, the dielectric is an insulator and charges are immobile, while J–R electroadhesives have higher conductivities, and charges are mobile. B) Two implementations of electroadhesives as electroprogrammable stiffness materials: electroadhesive clutches and electrobonded laminates. C) A classification of dielectric materials by relative permittivity and breakdown field strength. There is an inherent trade-off between the two quantities, and the maximum limit of any dielectric is $E_{bd}^2 k_d$. Traditional dielectrics are also subject to space charge accumulation, which can lead to screening of electrostatic attractive forces and unwanted residual attraction after removal of the applied voltage. D) Applications of electroadhesives in programmable stiffness technologies. These include haptic and virtual reality devices, orthotic exoskeletons, and grippers with tunable bending stiffness. C) Reproduced with permission.[20] Copyright 2019, Wiley-VCH. D) Top left image: Reproduced with permission.[20] Copyright 2020, Wiley-VCH. Top-right image: Reproduced with permission.[54] Copyright 2016, IEEE. Bottom images: Reproduced with permission.[52] Copyright 2017, Royal Society of Chemistry.

dominate when the bulk resistivity is greater than 10^{13} Ω cm.[48] The J–R effect, which is often utilized in electrostatic chucks in semiconductor manufacturing,[48,50] has not been utilized for electroadhesive stiffness modulation. As seen in Equation (2), J–R attraction can lead to larger electrostatic pressures at a fixed voltage since the interfacial gap g is often much smaller than the thickness of a dielectric film in a coulombic system,[50] thus making J–R adhesion potentially attractive for electrostatic clutches and laminates. J–R adhesion is also independent of dielectric material thickness and relative permittivity,[48] which could facilitate the use of dielectric materials with increased conductivity, such as aluminum nitride, in the next generation of electroadhesive programmable materials.

3.1.3. Implementations

Electrostatic clutches and electrically bonded laminates (EBLs) frequently use electroadhesive interfaces for stiffness modulation (Figure 3B). When loaded in tension, the holding force of an ideal electrostatic clutch or laminate is calculated using a canonical model for dry Coulombic friction and Equation (1)

$$F_{\text{hold}} = \mu F_{\text{C}} = \mu (n-1) \frac{A}{2} \varepsilon_{\text{o}} \left(\frac{k_{\text{d}} V}{d} \right)^2 \tag{3}$$

where μ is the coefficient of static friction between the electroadhesive surfaces and n is the number of stacked electrodes. If n is greater than or equal to three, the sandwiched electrode will be attracted to both the upper and lower electrodes present. Clutches are commonly used in robotic systems to control the transfer of force and mechanical energy through the body.[51] By coupling and decoupling springs in series and parallel, clutches allow selective control of stiffness and enable actuator designs that can leverage the passive dynamics of their structural materials for efficient performance.[53] Electroadhesives consume little power (typically around 1 μW due to leakage current through the dielectric), can be engaged and disengaged quickly (1–5 ms), and have been reported to produce holding stresses over 100 kPa, even up to 210 kPa at 300 V operation.[20,54,55] They are also lightweight, flexible, and easily integrated into fabrics or textiles, making them well suited for use in wearable devices. For example, Diller et al. developed electrostatic clutches for the stiffness selection of a wearable ankle exoskeleton,[51,54] while Ramachandran et al. and Hinchet et al. have developed similar tunable stiffness devices for wearable haptic feedback interfaces used in rehabilitation, virtual reality, and robot teleoperation.[20,21,56] Electroadhesive clutches have also been implemented in robots to control the stiffness of underactuated grippers and control the strength of modular systems.[57,58] Electro-bonded laminates are used to control the shape and stiffness of structural components, and their designs are often

quite similar to those of electroadhesive clutches. Unlike electroadhesive clutches, where two electrodes are selectively adhered using an electric field, EBLs are comprised of three or more selectively adhered layers for greater stiffness control. EBLs are well-suited for applications in which the bending stiffness of a structure must be dynamically changed. Example applications of stiffness modulation via electroadhesive laminates are shape-morphing and structural modification of airfoils,[59,60] as well as, dynamic vibration suppression in large structures and vehicles.[61–63] EBLs have also been used in applications where soft materials are programmed to stiffen for high-force operation. Examples include multilayered electroadhesive soft fingers with variable stiffness for high-force grasping,[52,64] stacked microscale electrostatic films for multifunctional assistive devices,[65] and origami-inspired electro-laminates that utilize zipping phenomena for both high-force and high-displacement operation in robotic actuators.[66]

3.1.4. Materials

Different materials have been used as dielectric films in electrostatic systems, and their electrical and mechanical properties play a critical role in determining the performance of the clutch or laminate. The maximum holding force produced by an electroadhesive device occurs at the breakdown field E_{bd}, or the electric field at which current flows through the dielectric. Breakdown often leads to local heating of the film and a rapid reduction in contact area, which can result in a decrease in the total electric field available to create electrostatic attraction, or even an unwanted separation of the clutch or laminate layers. Besides breakdown, there is a trade-off between k_d and E_{bd} that limits the performance of dielectrics.[67] Generally, as the relative permittivity of a dielectric material increases, its breakdown field decreases. Figure 3C shows that the maximum performance line that characterizes this trade-off is $E_{bd}{}^2 k_d$.[67] Mylar and Kapton dielectrics are inexpensive and readily available, but are limited by relatively low breakdown strength and low relative permittivity.[20,21] Other thermoplastic materials are closer to the empirical limit, including polymer-ceramic composites and fluoropolymers such as PVDF-TrFE-CTFE, which improve clutch adhesion by providing higher breakdown strengths and higher relative permittivity.[20,52] These materials, however, are expensive and can only be used in films thicker than 10 μm due to limitations of compatible blade-casting and molding methods.[20] Dielectric insulators with high breakdown strength and high relative permittivity such as alumina or silicon dioxide can be fabricated as micrometer or sub-micrometer thick films using approaches such as chemical vapor deposition or atomic layer deposition. These thin film fabrication approaches may enable higher holding forces at lower applied voltages, which would simplify the electronics used to control electroadhesive clutches. As the dielectric film becomes thinner, however, it is more susceptible to mechanical wear and cracking during cyclic operation. Highly worn clutches can wrinkle, crack, or delaminate from the dielectric film.[20] Wrinkles reduce the contact area between surfaces and cracks lead to short circuits, both of which lessen the friction produced at the interface and can result in device failure.[68]

Another phenomenon that has a profound effect on the magnitude of the electroadhesive force is screening due to space charge.[69] When a DC voltage is applied to the electrodes, space charges are injected into the dielectric layer and become trapped (Figure 3C). This results in a screening effect that reduces the strength of the applied electric field and the degree of electrostatic attraction at the interface. Furthermore, the screening effect due to the embedded charge persists even when the applied potential is turned off, leading to unwanted, residual electrostatic attraction (Figure 3C). The trapped space charges can persist for long periods of time, and the screening strength increases with electric field strength and the length of time that the DC voltage is applied.[70] To reduce the effect of space charge accumulation, an AC voltage can be used to rapidly switch the electrode polarity and constantly drive the space charges out of the dielectric layer. Hinchet and Shea accomplished this using an H-bridge to generate a symmetric, bipolar AC square wave input signal with a frequency of 10 Hz,[20] which greatly increased the clutch's peak holding force. Ramachandran et al. showed that reversing polarity can also greatly reduce the clutch's release time,[21] which is beneficial for precise control of electroadhesive systems. Despite these advantages, however, the use of an AC voltage signal causes a electroadhesive clutch or laminate to consume more power compared to DC activation due to constant charging and discharging of the electrodes.[20,21] While space charge accumulation occurs in all dielectric materials (both coulombic and J–R),[71] the use of higher voltages leads to higher amounts of trapped charge in the dielectric.[72] Also, dielectric materials prone to the formation of mechanical defects, such as voids, during the manufacturing process are more susceptible to failure due to space charge accumulation. The presence of surface contaminants or protrusions on the electrode surface prior to film deposition, or cavities within the dielectric material (e.g., bubbles) expedite partial discharge through small air voids, which effectively concentrate the applied electric field. When more charges become trapped, they can trigger these localized breakdown events, which, in turn, can lead to electrical treeing and the formations of short circuits that extend through the entire thickness of the dielectric layer.[72,73] To mitigate the effect of breakdown failure due to space charge accumulation, dielectric materials that require reduced activation voltages for operation and are less prone to defects, such as oxide-based films, could be implemented in an electroadhesive material system.[58]

Furthermore, all of the electroadhesive materials and systems discussed in this section utilize dielectric materials where Coulombic attraction dominates. Kim et al. recently demonstrated a new electroadhesive system comprised of ionoelastomers whose working mechanism is similar to the J–R effect.[74] This electroadhesive operated at low potentials with high force capacity, a 1 cm^2 electroadhesive pad produced 5 kPa of shear stress at 1 V, as the electric field was generated across a molecular-scale ionic double layer. Despite this impressive performance, the ionoelastomer material system suffers from minimum charging times of 1 s, which is among the slowest for electroadhesives with programmable stiffness. While the RC time-scale for charging of the ionic double layer is 60 ms, viscoelastic effects that occur during the charging process result in a slower response.[74] In all, such a system presents a new avenue

for electroadhesive programmable stiffness, where dielectric layers are removed altogether in favor of electro-switchable charged macromolecule layers that can be operated at significantly lower voltages without the potential for breakdown.

In general, electroadhesive clutches are often designed to achieve a prescribed stiffness change in only one planar direction, in response to a particular set of loads. However, some applications, including pneumatically driven, shape-morphing sheets,[7] may benefit from electroadhesive stiffness programming in multiple directions. When designing any adhesive system, the contact interface's planar geometry has a nontrivial impact on electroadhesive force capacity.[75] Therefore, future work should focus on investigating the relationship between electroadhesive force capacity and contact interface geometry in order to inform clutch designs where stiffness changes in different planar directions can be carefully assigned.

3.2. Electrorheological Materials

Electrorheological (ER) materials are materials in which the rheological behavior can be controlled using an externally applied electric field. In most implementations, a relatively large electric field (0.5–3 kV mm^{-1})[76] polarizes high permittivity dielectric particles dispersed in a lower permittivity insulating medium and aligns the dielectric particles with the electric field lines. The induced particle alignment increases both the viscosity of the material and its shear modulus. This modulus change is reversible and fast, on the order of milliseconds.[76] An ER material can contain an electrorheological fluid (ERF), whose insulating medium is a fluid, or an electrorheological elastomer (ERE), whose insulating medium is a cross-linked elastomeric polymer, as shown in **Figure 4**.[77] In order to achieve ER stiffening, there must be a mismatch between the relative permittivity of the dielectric particles and the insulating dispersal medium. Below, we review models that describe the shear resistance of both ERFs and electrorheological networks. We then describe how these materials are implemented in technologies with tunable stiffness and elucidate the effect of dispersed particle and dispersal matrix characteristics on overall performance.

3.2.1. Electrorheological Fluids

The shear resistance of an ER fluid with an insulating dispersal medium can be described in terms of a shear stress, τ, required for deformation. For any Newtonian fluid, the applied shear stress τ is related to viscosity η and shear strain rate by[78]

$$\tau = \eta\dot{\gamma} \tag{4}$$

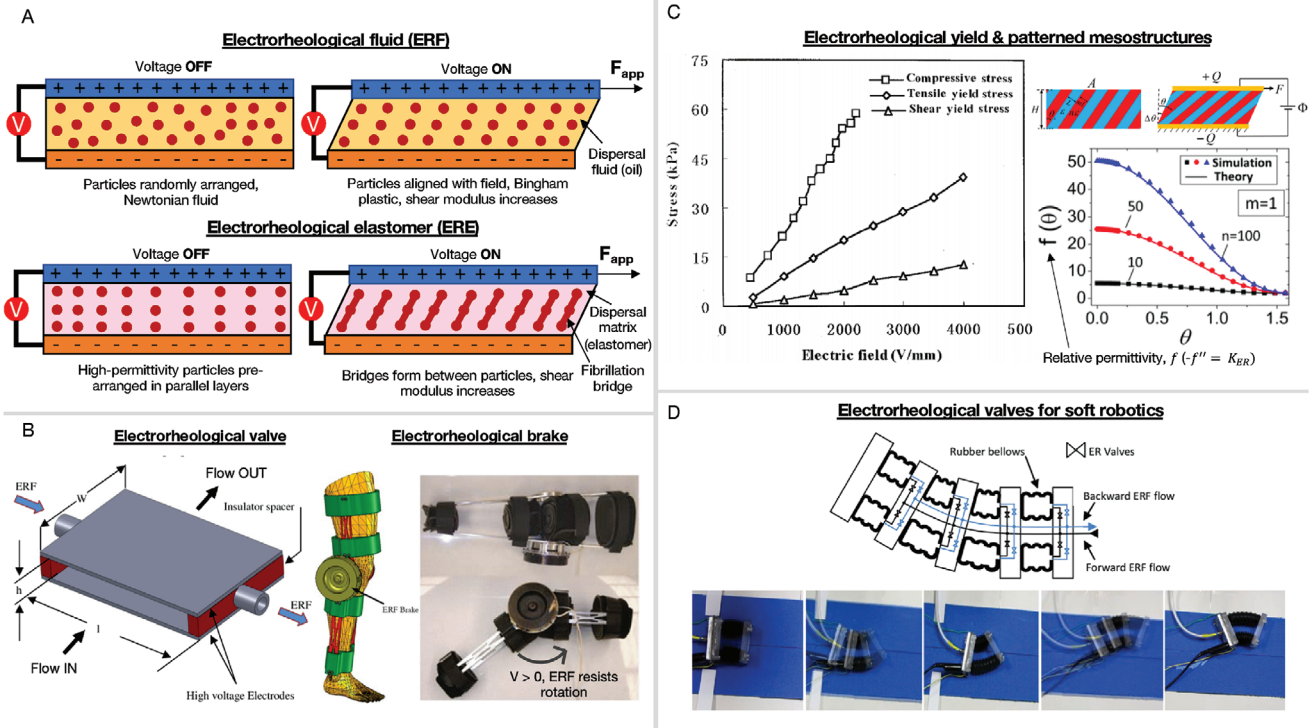

Figure 4. Electrorheological materials. A) Two types of electrorheological materials. Electrorheological fluids and electrorheological elastomers. B) Two implementations of electrorheological materials for electroprogrammable stiffness: Electrorheological valves and electrorheological brakes. C) Yield strengths of an electrorheological fluid versus applied electric field strength (left), and an electrorheological elastomer with a layered mesostructure (right). The material's relative permittivity changes with the angle of the layers. D) A soft robotic crawler with integrated ER valves. B) Left image: Reproduced with permission.[83] Copyright 2010, IEEE. Right and middle images: Reproduced with permission.[84] Copyright 2012, IEEE. C) Left image: Reproduced with permission.[84] Copyright 2002, American Physical Society. Right image: Reproduced with permission.[81] Copyright 2017, AIP Publishing. D) Reproduced with permission.[82] Copyright 2012, IEEE.

For an ERF, the viscosity changes when a field is applied due to enhanced electrically driven alignment of the dispersed particles. In this state, the ERF's behavior resembles that of a non-Newtonian Bingham plastic[79] and the total viscosity of an ERF, η_T can be described as

$$\eta_T = \eta Mn^{-\Delta} \tag{5}$$

where η is the absolute viscosity of the ERF, M_n is the Mason number, and Δ is a shear thinning exponent. The shear thinning exponent increases with electric field strength, and is usually between 0.68 and 0.91.[36,80] The Mason number relates the viscous and electrostatic forces in the ERF by

$$Mn = \frac{24\pi\eta_A\dot{\gamma}}{(\beta E)^2} \tag{6}$$

where η_A is the apparent viscosity of the dispersal of the ERF at the instant of electric field application. E is the strength of the applied electric field, and β is the dielectric mismatch parameter given by

$$\beta = \frac{k_p - k_f}{k_p + 2k_f} \tag{7}$$

where k_p is the relative permittivity of the of the dispersed particles and k_f the relative permittivity of the dispersal fluid.[36,80] From the total viscosity, the shear resistance due to both viscous and electrostatic effects can be calculated. As electric field strength increases, the Mason number decreases, which increases the total viscosity and shear resistance of the fluid. Therefore, the relative permittivity of the dispersed particles and dispersal is a critical design parameter to maximize the shear resistance change of any ERF material system.

3.2.2. Electrorheological Elastomers

An ERE is an electrorheological network that consists of high-permittivity particles distributed in an elastomer matrix, as shown in Figure 4A. Theoretical models for the performance of EREs have been developed and they predict the shear resistance of the solid material system as a function of the internal structure of the dielectric particles and the modulus of the elastomer matrix. The shear resistance τ of an ERE is

$$\tau = \overline{G}\,\Delta\theta + \frac{k_e\overline{E}^2}{2}K_{ER} \tag{8}$$

where $\overline{G}$ is the average shear modulus of the ERE, $\Delta\theta$ is the deformation angle of the ERE after a shear force is applied, k_e is the relative permittivity of the elastomer, $\overline{E}$ is the average electric field strength, and K_{ER} is the electrorheological coefficient of the system.[81] The electrorheological coefficient K_{ER} is a function of the permittivity and length ratios between the high-permittivity layers and the elastomeric dispersal matrix. By arranging columns of dielectric material in parallel strips, as shown in Figure 4C, Cao and Zhao predicted that K_{ER} can greatly increase.[81] If the angle between strips of dielectric material approaches zero, the ERE's electrostatic potential energy decreases. Thus, the shear stress required to deform the ERE structure to a fixed amount of shear strain with an applied voltage is greater than the required shear stress when the voltage is off. This theoretical, electrically driven enhancement in shear modulus could be achieved with the appropriate selection of elastomer and dielectric materials, but has yet to be proven experimentally.[81]

3.2.3. Implementations

Electrostatic valves and brakes frequently utilize electrorheological materials for stiffness change, as seen in Figure 4B. Flexible robots that use pressurized fluids for stiffness change often use electrically controlled solenoid valves to control fluid flow in and out of actuators.[86] Electrorheological valves have recently emerged as an alternative to solenoid valves, as they can sustain large pressures while minimizing the number of parts in a given robot design. ER valves consist of parallel electrodes with a dielectric spacing layer sandwiched between them and a slot that serves as the primary flow channel for the actuation fluid. An ERF channel then cuts perpendicularly through the middle of the primary flow channel. Therefore, when the ER valve is turned on, the stiffness of the ERF increases, blocking flow. An ER valve can sustain high pressures (e.g., greater than 170 kPa) when actuated below 5 kV to enable full actuation of a soft robot, while maintaining a mass below 10g for on-board operation.[85] Sadeghi et al. and Tonazzini et al. developed ERF valves for macroscale soft robots, including a segmented soft worm and a serial soft manipulator, respectively, which can maintain pressures up to 1 MPa with no leaks.[79,82] In these cases, the valves themselves did not deform, as their electrodes were made from rigid materials. Some soft robotic applications require full-body deformation, which has led to the development of flexible ERF valves. Zatopa et al. developed a flexible ERF valve with liquid metal electrodes for large-strain deformation of octopus-inspired soft robot actuators,[85] while Kim et al. developed ERF valves using SU-8 photoresist to enable flexible MEMS actuators for microrobots.[87] Similar electrorheological tunable stiffness designs are found in brakes and clutches, which are particularly attractive for wearable orthotic devices. While many orthotic devices are bulky and non-portable, Nikitczuk et al. developed a lightweight knee orthotic that utilizes a ERF brake for high stiffness change, which provides up to 172 N m of resistive torque when operated at 5 kV.[83,88] Wearable ER devices such as this knee orthotic and an ERF clutch developed by Chapuis et al. can be operated in MRI and fMRI devices, as they contain no magnetic components. ER tunable stiffness devices are preferred over similar magnetorheological technologies for biomedical use,[36] which are incompatible when an MRI must be used in concert with a resistive orthotic, as needed in human motor dysfunction studies.[89]

Magnetorheological elastomers (MREs) operate in a similar manner to ERFs and EREs, where stiffness changes are triggered in milliseconds by the alignment of magnetic particles

within an nonmagnetic fluid or matrix upon the introduction of a magnetic field.[32,33] However, the stiffness of an MRE can be programmed using an electromagnetic coil.[90–93] These materials have been used as vibration absorbers and isolators for structural components, such as cryogenic cooling systems for infrared imaging.[90] For example, Leng et al. programmed a stiffness change of 3.2 MPa in an MRE when it was subjected to a magnetic field produced by an electromagnetic coil.[93] This change was produced by a hybrid electromagnet, which contained permanent magnets and an electromagnet. While a stiffness change could be achieved by an electromagnet alone, it would require constant power to maintain the effect. By using a hybrid design, significant electrical power was only required to change the magnetic field strength, as the permanent magnets provided the nominal field.[90] While these MREs exhibited electroprogrammable stiffness, future work should focus on developing MREs for vibration suppression systems whose stiffnesses can be programmed using electromagnets alone, as permanent magnets add significant weight and design complexity.

3.2.4. Materials

The structure and properties of the dispersed particles and dispersal medium are critical to the performance of ER materials. First, higher volume fractions of high permittivity particles in any ER material will increase the degree of stiffness change, as densely packed particles can form more chains upon application of an electric field. The same result occurs upon increasing the size of the dispersed particles (which are normally 0.1–100 μm in diameter), however, increased particle sizes and concentrations result in reduced stiffening speeds due to sedimentation effects which prevent chain formation.[80,94] The dispersed particle shape also impacts the ER material properties, as irregularly shaped particles such as ellipsoids lead to increased chain formation in the material and greater stiffness change, but also slower response times compared to ER materials with spherical particles.[94] Typically, the dispersed particles have a relative permittivity greater than 10, and are comprised of low-conductivity materials such alumina, glass, PMMA, PVDF, titanium dioxide, and lead zirconate titanate.[80,81] The dispersed particles also have high breakdown strengths to avoid shorting within the ER material. The dispersal medium composition is also critical to device performance. The ER dispersal medium should have a lower relative permittivity than the dispersed particles and the viscosity should be low enough to enable dispersed particle motion and the particle bridge formation upon introduction of the electric field. Typical ER dispersal mediums include low-viscosity fluids with high breakdown strengths, such as castor oil, silicone oil, fluorinated polymers, and kerosene,[80] or elastomers such as poly(dimethylsiloxane) (PDMS).[81] Finally, pre-structure, or the ordered alignment, of the dispersed particles in any ER material system can greatly enhance the amount of stiffness change by geometrically promoting or inhibiting chain formation, which has also been explored for MR stiffness change systems.[32,33] Further investigation into the geometric arrangement of electrorheological layers in a material could lead to novel ER stiffening devices without extensive optimization of the constituent ERF or ERE components.

A notable phenomenon in ER materials is the shear yield effect, which leads to a drastic reduction of the ER stiffening effect upon the application of a critical shear stress.[95] Before a critical shear yield strength is reached, the viscosity of an ERF increases with increasing electric field strength. At the critical shear yield strength of the fluid, the ERF begins to behave like a Newtonian fluid, and its shear resistance drops significantly. Choi et al. showed that the critical shear stress value, τ_c, is proportional to E^2 when the applied electric field strength, E, is below a threshold value, E_c, and is proportional to $E^{3/2}$ when E is above E_c.[95] In practice, ER materials are implemented with operating field strengths below E_c to avoid reaching the critical shear yield strength.[79] Finally, while this section has focused on modulus enhancements of ER materials under shear, ER fluids have also demonstrated similar enhancements under tension and compression.[84] As a result, new ER stiffness mechanisms could program stiffness increases under multiple loading conditions, which would benefit applications with multiaxial loading.

3.3. Dielectric Elastomers and Electrohydraulic Materials

3.3.1. Dielectric Elastomers

When a large electric field is applied across two stretchable electrodes separated by an elastomeric core, the resulting electrostatic forces deform the core in directions both perpendicular and parallel to the applied field. The combined electrodes and core are called a dielectric elastomer (DE).[96] As a result of the deformation, the core provides a restoring force against the electrostatic forces, as seen in **Figure 5**. The pressure induced by the field is known as the Maxwell pressure σ, and can be calculated by

$$\sigma = \varepsilon_o k_d \left(\frac{V}{d}\right)^2 \tag{9}$$

where V is the applied voltage, d is the thickness of the dielectric layer, ε_o is the permittivity of free space, and k_d is the relative permittivity of the dielectric layer.[97] The Maxwell pressure is larger than the attractive coulombic force in solid-state capacitors because DEs also benefit from the in-plane repulsive forces generated from like charges within a single electrode. These in-plane forces increase the amount of mechanical work done by an electrical energy input and double the electrostatic pressure of a DE compared to a capacitor with rigid electrodes.[40,97] A widely used technique to control DE deformation is to pre-stretch the DE before adding the electrodes. When the DE is pre-stretched in one planar direction (for example, the lateral direction), and the electric field is applied across the thickness of the device, it deforms orthogonal to the initial pre-stretch (the longitudinal direction).[98] Pre-stretching is typically done with a rigid frame, but this requires additional rigid components that add significant fabrication complexity and limit integration with highly deformable technologies.[99]

Since the dimensions of the elastomer change after the field is applied, the bending, compressive, and axial stiffness of the structure will change. The degree of stiffness change is highly

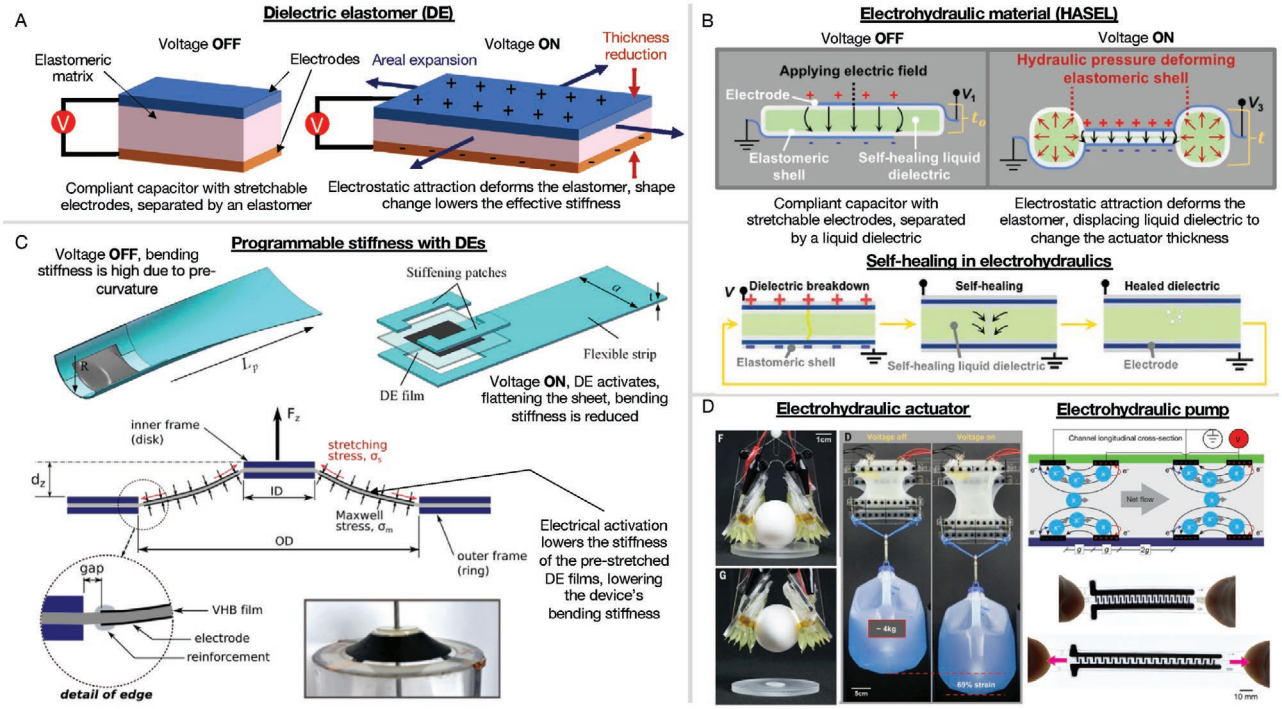

Figure 5. Dielectric elastomers and electrohydraulics. A) Working principles for dielectric elastomers (DEs). B) Working principles for electrohydraulic HASEL actuators, which have the ability to self-heal. C) A flexible, pre-stretched strip (top) with non-zero curvature capable of a stiffness reduction upon the activation of an embedded DE. A diaphragm configuration of DEs (bottom) whose bending stiffness decreases upon geometric changes triggered by electrical activation. D) Electrohydraulic material systems deployed as soft actuators with variable shape and stiffness, and as flexible pumps that control the pressure, shape, and stiffness of balloons. B) Reproduced with permission.[101] Copyright 2018, The Authors, published by AAAS. C) Top images (light-blue materials): Reproduced with permission.[112] Copyright 2017, IOP Publishing. Bottom images: Reproduced with permission.[106] Copyright 2016, IEEE. D) Left images ("Electrohydraulic actuator"): Reproduced with permission.[101] Copyright 2018, The Authors, published by AAAS. Right images ("Electrohydraulic pump": Reproduced with permission.[107] Copyright 2019, Springer Nature.

dependent on the final shape of the DE, which is determined by the shape of the electrodes, applied electric field strength, amount of pre-stretch, Young's modulus of the DE, and the relative permittivity of the elastomeric matrix.[35,100]

3.3.2. Electrohydraulic Materials

A material system comprised of two conductive electrodes covering an elastomeric shell filled with a dielectric liquid (DL) whose internal pressure increases with increasing applied electrical potential is known as an electrohydraulic material.[101–104] As the electrodes are attracted to one another, the dielectric liquid is displaced by Maxwell pressure, causing the elastomeric shell to strain and the effective stiffness to increase, which continues through pull-in. In other words, the system functions as a self-contained electrohydraulic pump, which increases the pressure of the internal dielectric liquid to change the overall shape and stiffness of the material.

All dielectric materials (DEs and DLs) are susceptible to pull-in, or a non-linear snap-through transition when the electrostatic attraction between the electrodes exceeds the restoring force of the elastomer matrix or shell. For DEs, pull-in increases the likelihood of breakdown and permanent damage to the material. For DLs, pull-in also leads to breakdown, but shorts are quickly filled in by the surrounding liquid.[101] This electrical self-healing phenomenon (seen in Figure 5B) allows the DL to survive numerous breakdown events without damage, enabling the application of higher electric fields and, in turn, higher amounts of Maxwell pressure within the material compared to DEs.

3.3.3. Implementations

Dielectric elastomers and electrohydraulic materials operated at high voltages undergo changes in stiffness due to their ability to achieve significant changes in shape. For example, an activated DE can reduce its axial and bending stiffness as the applied voltage increases length and decreases thickness. The axial stiffness, S_{DE}, of a DE sheet constrained to extend in only one planar direction after a voltage, V, is applied, can be calculated by[108]

$$S_{DE} = S_o - \frac{\varepsilon_o k_d w V^2}{lt} \tag{10}$$

where S_o is the stiffness of the DE sheet with no voltage applied, and w, l, and t are the width, length, and thickness of the deformed DE sheet. While all DEs undergo a stiffness reduction due to geometric effects, the specific number and configuration of DEs will determine the final degree of reduction and

whether or not the axial or bending stiffness is affected. Two common configurations for DE programmable stiffness devices include: 1) a cantilever beam, or 2) a diaphragm. The use of the cantilever beam configuration for DE stiffness change was first implemented by Pelrine and Kornbluh, who achieved a 10× reduction in the bending stiffness of a planar DE.[109] Henke et al. utilized the same DE configuration to reduce the bending stiffness of metal/elastomer composite beams by two orders of magnitude via the geometric reduction of moment of inertia upon electrical activation.[110] Similarly, Carpi et al. demonstrated a DE-based, beam-shaped, programmable stiffness device for a lightweight, active hand orthotic.[111] The DE device blocked the motion of a patient's fingers in the de-activated state, while electrical activation systematically increased the DE's length and width to reduce bending stiffness, allow for selective motion, and train the patient to follow specific finger trajectories during rehabilitation. In these implementations, the DE cantilevers were planar sheets before activation. Li et al., however, demonstrated a DE programmable stiffness beam whose initial state was a pre-stretched, curved beam, which relaxes to a flat sheet upon the application of high voltage.[105,112] The pre-stretched, curved shape resembled that of a monocot leaf, whose pronounced curvature lead to an increased bending stiffness, and the ability to stand under its own weight without collapse. An applied voltage allows relaxation from a pre-stretched state, which is common in diaphragm-shaped DEs. Dastoor et al. and Orita et al. implemented multiple, pre-stretched DE sheets arranged in a conical geometry, whose stiffness was reduced by the electrical relaxation of that pre-stretch.[106,113] Since pre-stretch increases the de-activated axial and bending stiffness of a DE, DEs with pre-stretched films can achieve larger stiffness reductions compared to those that are not pre-stretched.

The use of dielectric liquid for self-healing soft robotic actuators was introduced by Acome et al., where the authors developed hydraulically amplified self-healing electrostatic (HASEL) actuators.[101] Electrostatic MEMS actuators driven in dielectric liquids had been previously explored,[114–116] but HASEL actuators were the first implementation of a soft, macroscopic, electrohydraulic actuator. The presented HASEL actuators were formed into toroidal or planar designs, depending on the desired application, both of which are shown in Figure 5B. Each HASEL actuator was comprised of conductive PAM hydrogel electrodes, an elastomeric shell molded using PDMS, and a dielectric liquid of vegetable-based transformer oil. A single HASEL actuator can produce 0.75 kPa of actuation stress and 15% strain at 11 kV. The actuator can also operate after 50 breakdown events and can be cycled over 1 million times when lifting 150 g without failure. Both the total output force and actuation strain directly scales with the number of toroidal HASEL actuators operated in a stacked configuration.

A HASEL's electrode area is directly proportional to axial stiffness change, while electrode area and compressive stiffness change are inversely proportional. Since Maxwell pressure is not directly related to electrode area, the electrode size was designed to control the amount of dielectric liquid displaced by the applied electric field. When the electrode area was significantly smaller than the overall area of the toroidal elastomeric shell, a small amount of liquid dielectric was displaced, leading a greater degree of internal pressurization and stiffness change, at the expense of lower actuation strains. When the electrode area was increased, more dielectric fluid was displaced, which decreased the pressure and stiffness change of the DL but allowed higher actuation strains.[101] Similar to electrorheological materials, it is important to consider the desired type of stiffness change when designing a HASEL actuator's geometry.

By changing the shape of the electrodes or operating different numbers of HASEL actuators in series or parallel, the shape and stiffness change of an electrohydraulic material can be specifically controlled. Kellaris et al. utilized this phenomenon by implementing HASEL actuators in a Peano-fluidic actuator to achieve large linear deformations without any pre-stretch or rigid components.[102] When a voltage was applied to a connected array of rectangular, electrohydraulic pouches, the induced Maxwell pressure displaced the liquid dielectric fluid, causing each pouch to contract and stiffen. As each pouch contracts, the electrodes of each pouch unit get progressively closer together, leading to an electrostatic zipping effect that results in large amounts of linear deformation. One Peano-HASEL unit could achieve a 10% strain with an applied load of 20 g at 10 kV operation. As predicted by Equation (9), the amount of mechanical stiffness change for each Peano-HASEL array increased with increasing electric field strength (as each pouch can be inflated to a larger internal pressure), and can be scaled up further by adding more Peano-HASEL units in parallel.[102]

HASEL and Peano-HASEL designs have inspired the development of other electrohydraulic actuators for different applications. These include a soft gripper driven by electrohydraulic pouch units that can grasp delicate objects,[117] an active electrohydraulic actuation plate with asymmetric electrodes to control the position of surface objects,[118] and a proboscis-inspired electrohydraulic transducer that can stiffen or soften to produce coiling motions.[119] Leroy and Shea recently introduced hydraulically amplified taxels (HAXELs), which are millimeter-scale HASEL actuators for virtual reality and augmented reality systems. Each HAXEL can achieve strains up to 500 microns and forces up to 300 mN, and can be tightly packed into flexible, cutaneous haptic feedback arrays that can be worn by a user.[120] Recently, electrohydraulic materials have been integrated into other electroprogramming methods, like electroadhesion. For example, Taghavi et al. developed an electrohydraulic zipping actuator with an electro-laminate design that can change its stiffness to produce large displacements or large output forces through the use of a dielectric liquid to enhance electrostatic attraction between layers without breakdown.[66]

Electrohydraulic pumps have also been directly integrated into soft actuators for electroprogrammable stiffness change. Electrohydraulic pumping systems use an applied electric field to drive ion transport, which, in turn, moves a working fluid into a soft cavity. As a result, the fluid pressurizes the cavity, increasing its compressive stiffness while consuming little power. While there are many types of electrohydraulic pumping systems,[121] Cacucciolo et al. recently designed a flexible electrohydrodynamic pump that can be fabricated directly into an elastomeric bending actuator. Each pump used a charge-injection mechanism to drive a dielectric fluid from an attached reservoir to a soft finger, enabling untethered pressurization and stiffness change without the use of external compressors.[107]

Figure 5D shows the charge-injection mechanism. When a large electric field was applied, electrons from the cathode tunneled directly into the dielectric liquid, and ions were generated via field emission. These ions were accelerated by the electric field until they discharge at the anode, transferring momentum to neutral liquid molecules to create a net flow. When a voltage of 8.25 kV was applied to a bending actuator with the internal electrohydraulic pump, it was pressurized and could bend more than 40 degrees from its rest position. Similarly, HASEL actuators have been implemented in compliant pumps to increase the stiffness and change the shape of a material system. For example, Wang et al. developed an artificial circular muscle via radially arranged high-strain Peano-HASEL actuators which could increase the pressure of a soft cavity from 1.30 to 2.73 kPa upon introduction of a 10 kV voltage.[122] Overall, while HASELs and electrohydraulic materials have great potential to replace pneumatic or hydraulic materials with programmable stiffness, their operating voltages must be decreased for true compatibility with untethered electronics systems.

3.3.4. Materials

The material composition of DEs and electrohydraulic systems directly influences the degree of shape and stiffness change they undergo. Common material candidates for compliant electrodes are films containing carbon black,[123] carbon nanotubes,[124] graphene,[125] and patterned metal traces.[126,127] Many of these materials can be difficult to reliably integrate into existing manufacturing techniques, which leads to electrical breakdown at high strains and voltages.[128,129] In one improvement, Keplinger et al. developed a stretchable ionic conductor for high-voltage and high-frequency operation of DEs.[129] The conductors were comprised of a polyacrylamide hydrogel in series with an insulating elastomer, sandwiched by two electrodes. When a potential was applied across the electrodes, an electrical double layer was formed at the electrode/electrolyte interface. The electrical double layer acted as a capacitor, which was in series with the electrolyte/insulator interface that acted as another capacitor. Since the charge separation of the electrical double layer is on the order of nanometers, its capacitance is significantly greater than that of the elastomeric matrix. As a result, the electrodes can apply high voltages (upward of 10 kV) without causing damage or breakdown in the hydrogel (which only saw a small voltage drop around 1 V).[128,129] It is notable that DEs used in programmable stiffness systems can reach minimum stiffnesses close to or equal to zero, without requiring contacting electroadhesive elements.[106] However, the minimum stiffness of a DE can only approach zero as the applied voltage increases and the thickness of the DE film decreases, which become susceptible to tearing and electrical breakdown caused by pull-in.[106,113] Furthermore, the initial, de-activated voltage of a DE can be increased by increasing mechanical pre-stretch, which can be relaxed by electrical activation. Nonetheless, pre-stretching requires a rigid frame to maintain tension in the DE film, and can lead to unwanted stress concentrations between that frame and the soft elastomer. Therefore, it would be beneficial to maintain high pre-stretch without the use of a rigid frame. A few different methods have been explored to accomplish this, including the use of interpenetrating polymer networks, ultraviolet radiation polymerization for DE fabrication, and chemically modified thermoplastic elastomer (TPE) gels.[130–132]

Common fluids used as DLs include oils and fluorinated solvents, which have high breakdown strengths and are also used as the dispersal medium in ERFs.[101,107] A few considerations should be taken into account to improve the performance of DE and electrohydraulic materials. First, the operating voltages of DEs and electrohydraulic materials are high (up to ≈30 kV).[101] In order to reduce operating voltages while maintaining the ability to achieve stiffness change and high actuation strain, researchers have suggested the use of insulating materials with increased relative permittivity via the addition of fillers such as copper phthalocyanine oligomer, or actuator geometries comprised of elastomeric shells with reduced thickness, which can be enabled by high-resolution stereolithographic 3D-printing.[40,102,133] O'Neill et al. recently demonstrated the rapid 3D printing of a fully encapsulated, soft HASEL actuator that acts as an artificial hydrostat. While this material system was able to reproduce the characteristics of traditional HASELs, further work is required to develop additive manufacturing technologies with improved spatial resolutions, which, in turn, could decrease the driving voltage for a 3D printed equivalent.[134] As the thickness of elastomeric shells decrease, however, they are at increased risk of puncture due to electric breakdown events.[102] To avoid this, developing high-toughness elastomers which excellent dielectric properties is crucial to improving the structural integrity of next-generation electrohydraulic materials.

Furthermore, the MEMS community has provided critical insights that could reduce the driving voltage of HASELs and electrohydraulic materials. First, Chang and Maharbiz introduced microfluidic valves which operate in water and operate at 15–20 V to control fluid flow without pneumatics.[135] By using water as a dielectric liquid, which has a high relative permittivity, the amount of voltage required to reach electrostatic pull-in was very small compared to the kilovolts required for HASEL actuation. The authors mitigated electrolysis and prevented the appearance of short circuits by coating a metal electrode in a oxide layer, improving the breakdown strength of the coating, and using an AC voltage signal.[114,135] While an oxide layer was effective at preventing short circuits, any insulating material with a breakdown strength higher than that of water should be sufficient, such as silicon nitride.[115,136] The choice of water as the dielectric liquid could reduce the voltage of HASELs or electroadhesives, but the electrodes would have to be close enough (less than the Debye length) in order to generate an electrostatic force that is not quickly screened.

4. Electroprogrammable Stiffness via Electrically Driven Phase Change

4.1. Electrochemistry

In an electrolytic cell, an electric current drives chemical changes through redox reactions at an anode (oxidation) and cathode (reduction), where electrons are conducted from

the anode to the cathode through a voltage source while ions balance the charge by conducting through an electrolyte that connects the anode and cathode. Electrochemistry has been extensively used to produce chemicals, manufacture and modify materials, and realize energy sources.[137–141] Here, we discuss how electrically driven chemical changes have been used to program stiffness changes in ionoprinted hydrogels, electroplastic elastomer hydrogels (EPEHs), and electrochemically reconfigurable microlattices. Finally, we detail the implementations of these electrochemical materials in reconfigurable actuators and self-assembling structures, and how material selection and properties are critical to realizing fast, large, and programmable stiffness changes in electrochemical systems.

4.1.1. Ionoprinted Hydrogels

Ionoprinting is a process where an electrical input is used to release metal ions into a hydrogel, which increases the number of local crosslinks and hydrogel stiffness. Ionoprinting was first demonstrated by Palleau et al. to electrically pattern stiffness gradients and topographical features in sodium polyacrylate (pNaAc) hydrogels.[142] In this process, a anode, typically copper, is oxidized to produce multivalent ions (Cu^{2+}) which diffuse and displace monovalent counterions (Na^{+}) attached to functional groups (carboxylic) on the polymer backbone, as seen in **Figure 6**. The multivalent ions associate with multiple functional groups to increase the crosslink density and gel stiffness. These ionic crosslinks cause the gel to change color and are visibly stable in the gel for months when placed in a water bath. Ionoprinting requires a small potential, 2–3 V, and can occur in a few seconds when the diffusion distances are small. The total number of functional groups available has a large impact on the ionoprinted feature depth and the final material stiffness. Palleau and collaborators reported a 279 kPa change in compressive modulus between ionoprinted and virgin pNaAc gels. The imprint depth increased as the applied voltage increased until about 10 V due to ion saturation in the gel. Ionoprinting is also reversible. To remove the cupric ions, the ionoprinted hydrogel was immersed in ethylenediaminetetraacetic acid (EDTA) for 4 h to allow for chelation, or the complexation of the cupric ions with the EDTA's multidentate ligands. After 4 h, the gel softened and returned to its original stiffness. While Palleau et al. pioneered the ionoprinting technique, other researchers have built upon this work to create different types of ionoprinted hydrogels. To date, cations of copper, aluminum, titanium, iron, vanadium, calcium, and zinc have been successfully ionoprinted in different types of hydrogels containing functional catechol, phosphate, and hydroxyl side groups.[142–148] For example, inspired by the composition of mussel secretions critical to wet adhesion, a dopamine methylacrylamide (DMA) hydrogel was prepared with network-bound catechol, which was capable of forming strong complexes with metal ions of various types, including aluminum, titanium, copper, iron, and zinc.[144,149] By immersing the gel in solutions of varying pH, Lee and coworkers could control the stoichiometry of the ionoprinted catechol–metal ion complex, which affected local crosslinking densities at ionoprinted sites and enabled reversible actuation.[145] Ionoprinted hydrogels fabricated with novel stimuli-responsive materials and embedded with different types of metal cations can achieve different degrees of stiffness change and swelling behavior.

4.1.2. Electroplastic Elastomer Hydrogels

An EPEH is a material whose stiffness can be modified by electrochemically changing the valence of metal ions dissolved in the hydrogel matrix. In the original inception by Calvo-Marzal,[150] a permanently crosslinked poly(ethylene glycol) diacrylate (PEG-DA) hydrogel was immersed in an electrolyte solution of iron chloride and citric acid for 20–48 h and became infused with Fe^{2+} and Fe^{3+} ions. When the hydrogel was saturated with Fe^{3+} ions, the number of local crosslinks in the material increased due to the geometric compatibility of the cations and the carboxylate groups in the gel's polymer backbone, leading to an increase in stiffness. When a reductive potential of –0.8 V was applied to the stiff gel for 18 h and placed in an electrolyte bath, the Fe^{3+} ions were reduced to Fe^{2+}. Since the shape of the Fe^{2+} ions were weakly compatible with the gel's carboxylate backbone, the number of local crosslinks went down, and the gel softened. This electrochemically driven interconversion between iron cation oxidation states (and thus, soft and stiff mechanical states) is reversible; an oxidative potential of 1.2 V applied to the weakly crosslinked (soft) hydrogel for 14 h will oxidize Fe^{2+} to Fe^{3+} and increase the gel modulus. Through this process (Figure 6), Calvo-Marzal reported changes in compressive modulus up to 0.4 MPa.[150] Similarly, other metal cations have been implemented in EPEHs. Harris et al. utilized the Cu^{2+}/Cu^{+} transition to achieve 2.89 MPa changes in compressive modulus, a significant improvement over the Fe-EPEH.[151] The Cu-EPEH also has a shape memory effect due to the redox properties of copper. If a flexible Cu-EPEH specimen was fabricated with Cu^{+} ions, it could be formed into a new shape and stiffen to lock-in that shape after undergoing oxidization. Complete reversibility between hard and soft states for both the Fe-EPEH and the Cu-EPEH was not possible using electrochemistry alone. Finally, the speed and degree of modulus enhancement has been increased by incorporating graphene oxide (GO) into Fe-EPEHs, which enabled thinner specimens with greater toughness. Auletta et al. reported Fe-EPEHs incorporated with GO capable of 2 MPa electrochemically driven modulus changes in as little as 30 min at reductive potentials of –0.8 V, compared to 12–16 h for Fe-EPEHs without GO.[152] Overall, ionoprinted hydrogels and EPEHs show the potential of electrolytically driven metal redox reactions in polymer gels to realize materials with programmable stiffness.

4.1.3. Electrochemically Reconfigurable Microlattices

Architected materials can achieve a wide variety of desired mechanical behaviors through the sub-structural patterning of mechanical elements, such as slender beams and plates.[153,154] Most architected materials have a fixed internal structure, but a new class of architected materials can reconfigure their macroscopic shape through stimulus-driven stiffness modulation of their mechanical sub-elements.[155] One notable type

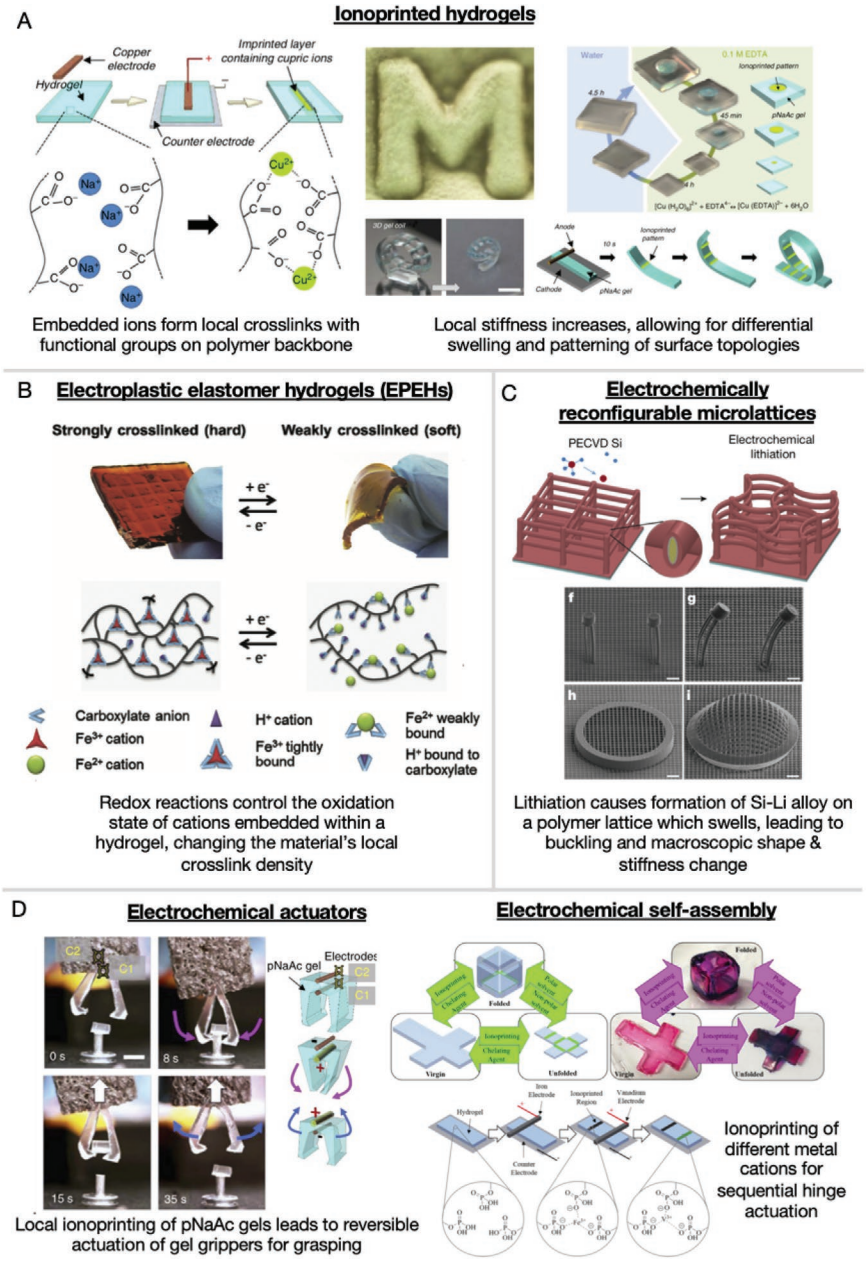

Figure 6. Electrochemistry. A) Schematic describing the process of ionoprinting for hydrogels. When metal ions are released into a hydrogel, they associate with functional groups on the polymer backbone, increasing the crosslink density and gel stiffness (left). This process caused the gel to change color and stiffness changes can be produced with high spatial resolution to recreate the surface features of a US penny (middle). Ionoprinting is reversible, as metal ions can be removed with immersion in EDTA solution (right). Selective areas of a gel can be ionoprinted and stiffened for precise actuation upon gel swelling (right). B) Schematic describing the stiffening and de-stiffening of electroplastic elastomer hydrogels. When a reductive potential was applied to the gel, integrated Fe^{3+} ions were reduced to Fe^{2+}, and the number of local crosslinks in the material decreased due to the geometric incompatibility of the cations and the carboxylate groups in the gel's polymer backbone, causing it to soften. By applying an oxidative potential, the electrochemically driven iron cation interconversion can be reversed, oxidizing Fe^{2+} to Fe^{3+}, increasing the gel's modulus. C) Photos of electrically driven swelling of polymer microlattices. When a constant current was applied to a Si-coated microlattice and a Li counter electrode, Li^{+} was reduced to convert Si to a Li–Si alloy, changing the stiffness of individual beams and the entire microlattice structure (top). This was utilized to produce stiffness changes that lead to bending deformations in individual beams, resembling soft actuators, and geometric configuration changes that change planar lattices into 3D shapes (bottom). Electrochemically reconfigurable grippers actuated via ionoprinting (left). When upper and lower sections of the gel are alternatively ionoprinted, a fingered gripper can open and close until the gel becomes saturated with cupric ions. Electrically driven stiffness change of an ionoprinted gel sheet via electrochemically driven geometric assembly into a 3D structure (right). By ionoprinting a gel with metals ions of differing reductive potentials, it can be sequentially actuated when placed in a reducing agent, such as ascorbic acid. A) Reproduced with permission.[142] Copyright 2013, Springer Nature. B) Reproduced with permission.[150] Copyright 2012, American Chemical Society. C) Reproduced with permission.[156] Copyright 2019, Springer Nature. D) Left part: Reproduced with permission.[142] Copyright 2013, Springer Nature: Right part, top: Reproduced with permission.[148] Copyright 2015, The Authors. Right part, bottom: Reproduced under the terms of the CC-BY Creative Commons Attribution 3.0 Unported license (https://creativecommons.org/licenses/by/3.0).[146] Copyright 2016, IOP Publishing.

of stimulus-driven architected material is an electrochemically reconfigurable microlattice, first reported by Xia et al.[156] In this example, a polymer lattice was first 3D printed using two-photon lithography and configured to be a square grid comprised of slender struts with elliptical and circular cross-sections. Next, a thin nickel layer was sputtered on the polymer followed by silicon deposited via plasma-enhanced chemical vapor deposition. Silicon (Si) was the anode in this system, selected for its high volume expansion (up to 300%) and capacity when alloyed with lithium (Li), which also makes it attractive for Li-ion batteries.[157] When a constant current of 5 μA was applied to the microlattice (submerged in electrolyte) and a Li counter electrode, Li^+ reduced to convert Si to a Li–Si alloy on the beams. The accompanied volumetric expansion and phase change modified the stiffness of individual beams, whose axial length and cross-sectional areas both increased. After large expansions, the beams buckled and changed the macroscopic lattice configuration. The 5 μA current achieved maximum swelling and beam buckling in an hour and the process was reversed through electrochemical de-lithiation (a negative current relative to the lithiation step), although the total number of cycles will be limited by Si fracture and electrolyte consumption, as observed in batteries. While this buckling behavior has been previously reported in lithiated silicon nanowires and edged-honeycomb patterns,[158,159] Xia et al. displayed its first use as a design tool for coordinated shape and stiffness change.

4.1.4. Implementations

Since electrochemical processes can lead to local, reversible changes in mechanical stiffness within a bulk material, they have been used to reconfigure actuators and self-assemble structures. For example, Palleau et al. demonstrated the use of an ionoprinted pNaAc hydrogel in a reconfigurable gripper.[142] When sections of the gel were ionoprinted, they became stiff and served as an exoskeleton that held the gel's shape. When the ionoprinted gel was placed in an organic solvent for 30 min, such as ethanol, it underwent volumetric contraction, and reconfigured its shape due to the increased rate of water expulsion in the ionoprinted sections and the stiffness mismatch between ionoprinted and non-ionoprinted regions. To regain the previous shape, the actuated gel was placed in water for 20 min, and its volume expanded until the original configuration was reached. This hydrogel was, therefore, capable of electroprogrammable, two-way shape memory: The gel remembered the initial ionoprinted shape and could be induced into a second shape by solvent introduction. The degree of shape change due to solvent immersion can be controlled by changing the ionoprinting time, which determines the number and depth of the embedded cupric ions and the stiffness of the ionoprinted regions. Palleau et al. demonstrated two different ionoprinted grippers whose operating principles take advantage of different ionoprinted gel behaviors. First, the authors demonstrated a triangular, ionoprinted gripper with two fingers, whose actuation mechanism was based on induced stresses caused by alternating ionoprinting of the upper and lower portions of the gel, as shown in Figure 6D. However, after three actuation cycles, the upper and lower regions of the gel become saturated with cupric ions, and it could not be cycled again. To solve this issue, Palleau introduced a second ionoprinted gripper that relied on differential swelling of the stiff/soft regions of the gel. Stiff, ionoprinted lines were first patterned on the back of the x-shaped device. When the gel was placed in ethanol, the ionoprinted regions expelled liquid faster than the non-ionoprinted regions, which led to uniform curvature along the stiffened lines. This caused all of the fingers to bend, which then gripped a variety of small, lightweight (0.1–1 g) objects. The ethanol/water actuator "strokes" could be repeated more than 10 times with only moderate hysteresis.

A hydrogel can also be electrochemically actuated via ionoprinting and the overall stiffness changed due to geometric modification. For example, Baker et al. ionoprinted a 2D hydrogel sheet with cations of different metals to sequentially assemble it into a 3D structure after immersion in a reducing agent.[146] As seen in Figure 6D, the lid of the hydrogel cube was connected to the rest of the cube body with a hinge ionoprinted with Fe^{3+} cations, while the rest of the cube pattern had hinges ionoprinted with V^{3+}. After ionoprinting the hinge locations for a sustained period of time (≈5 min), the 2D pattern formed its 3D cube shape. To sequentially unfold the cube, it was placed in a mild reducing agent (ascorbic acid), which selectively reduced the Fe^{3+} cations to Fe^{2+} due to their increased reduction potential compared to the V^{3+} cations, which were unaffected. As a result, the lid opened, and the cube was placed in a non-polar solvent to unfold the other hinges, bringing it back to a flat configuration. While Baker displayed a two-step, sequential actuation process, ionoprinting hydrogels with metals cations of different types could enable complex, multistep structural assemblies at a variety of folding rates,[144,146] and fine control of stiffness via shape change. Overall, for all types of electrochemical materials, significant advances must be made in order to greatly reduce the stiffening time, which would enable their use in applications that require high-speed operation.

Finally, ionoprinting techniques with novel stimuli-driven hydrogels have been combined to create novel reconfigurable actuators and self-folding structures that can be precisely controlled with a wide variety of stimuli. Morales et al. demonstrated heat-driven, reversible formation of complex 3D shapes by externally ionoprinting a thermoresponsive PNIPAm/pNaAc gel composite.[160] This bilayer hydrogel composite was responsive to both solvent immersion (ethanol) and heating, and formed specific shapes dictated by ionoprinted hinges. Similarly, Baker et al. demonstrated a NIPAM/MOEP ionoprinted hydrogel which changed shape when thermally cycled above and below its lower critical solution temperature (LCST).[161] The number of material systems that integrate ionoprinting and stimuli-responsive hydrogels will increase as more gels with novel properties continue to emerge, including those that can be actuated by light or pH combined with electrical input.[162]

4.1.5. Materials

For electrochemical systems, material selection greatly impacts the degree and reversibility of stiffness change, the mechanical behavior, and the speed of material programming. In ionoprinted hydrogels, stiffening only occurs with the appropriate

metal/hydrogel combination. For example, cupric ionoprinting was possible with pNaAc (polyelectrolyte) gels but not possible with a pure acrylamide gel that did not contain fixed sodium counterions, which have a lower binding affinity and get replaced by injected cupric ions.[142] Metal/hydrogel combinations that have been successful include iron/acrylic and vanadium/acrylic, which leverage phosphate and hydroxyl groups in the polymer backbone, and a variety of metals and a DMA/catechol gel. The rate and degree of actuation depends on the diffusivity and mobility of metal ions that are ionoprinted. Titanium (Ti^{4+}) cations, for example, demonstrated the highest stiffness change, actuation rates, and bending angles in a metal-catechol DMA gel actuator as they formed the strongest complexes with the catechol side groups.[144] Ionoprinted Ti^{4+}, however, cannot be fully removed via EDTA immersion since the cations are tightly bound to the catechol network. As a result, there are clear trade-offs between degree of stiffness change and reversibility for ionoprinted hydrogels.

Similar to ionoprinting, metal cation and polymer functional group selection critically affects the reversibility and final degree of stiffness change in EPEHs. While ionoprinted hydrogels display two-way shape memory, Cu-EPEHs can only achieve one-way shape memory, as stiffness changes cannot be localized to individual sections of the gel.[151] EPEHs, however, do not require a chemical input to reverse stiffness changes, as the necessary ions are stored in the gel matrix. As a result, the minimum time required for material programming is greatly reduced compared to ionoprinted hydrogels, which must be immersed in EDTA to remove stiff features. In some cases, especially at electrode-hydrogel interfaces, cations can also form permanent cross-links which detrimentally affect the reversibility and speed of stiffness changes due to reduced ion mobility.[151] Finally, the degree of stiffness change in EPEHs are affected by environmental factors, particularly oxidation at air interfaces which reduced the degree of softening.[150] Despite being faster than ionoprinted gels, future work in EPEHs should focus on increasing the speeds of the oxidation-reduction reactions necessary for stiffening and increasing the reversibility of electrochemical stiffening via environmental shielding for applications that require stiffness changes in real time.

When considering electrochemically reconfigurable microlattices, the choice of anode material, alloying element, presence of material defects, and selection of alloying voltage determine the final anode phase and mechanical response of the system. First, there are a large variety of electrodes that can be electrochemically swollen to drive stiffness change, including many intercalation, conversion, and alloying electrodes used in batteries.[163] The chemical composition, kinetics, and mechanical response of these materials have been extensively studied in battery literature. Titanium-oxide-based intercalation electrodes, for example, undergo small volume changes (2–3%) during lithiation, but can be reversibly cycled thousands of times.[163] Alloying elements like Si, germanium (Ge), aluminum (Al), and tin (Sn) undergo large volume expansions (>100%), which necessitate nanoscale lattice dimensions to reduce large strain-induced fracture.[164] During delithiation above 0.6 V in the Si nanolattice, the underlying polymer began to fracture, so cut-off voltages had to be kept below 0.6 V to enable long-term shape and stiffness change of the material system. Next, material defects, which occur due to residual stresses in individual struts or misalignments at strut junctions, locally influence the stress distribution of lattice beams and can be leveraged to precisely control the macroscopic shape and stiffness of the overall system.[156] Material defects also make beams more susceptible to fracture or delamination. The low degree of reversibility (due to fracture) and large internal stress requirement for actuation is a notable weakness for electrochemical systems with large volume expansions. Future work can take advantage of alternative battery materials to develop lattices whose shape and stiffness can be programmed reversibly for many cycles.

4.2. Electrothermal Materials

When an electric current passes through a conductive material, electric energy is converted to heat via resistive losses in a process commonly referred to as Joule (or ohmic) heating.[165] The resulting heat can be used to induce stiffness change by heating the material above a critical temperature and inducing a phase change. Here, we classify all electrically heated materials whose stiffness can be programmed via a phase transition as electrothermal materials. For the purpose of this progress report, we will focus on the electrothermal materials that undergo an electrically induced phase change at temperatures below 100 °C. The five main classes of electrothermal materials that have been used to realize tunable stiffness are summarized in **Figure 7**: thermoplastic elastomers (TPEs), liquid-metal-embedded elastomers (LMEEs), shape-memory alloys (SMAs), liquid crystal elastomers (LCEs), and thermoresponsive hydrogels.

4.2.1. Thermoplastic Elastomers and Shape Memory Polymers

A thermoplastic is composed of chemically independent macromolecule chains that soften and deform as a fluid after heating.[166] Thermoplastics are extremely common, and their ability to soften upon heating is critical to many manufacturing processes, such as injection molding and thermoforming. The reversible nature of the thermoplastic phase transition, however, has also gained significant interest for realizing stiffness change. The critical phase transition temperatures for a thermoplastic are the glass transition temperature (T_g) and the melting temperature (T_m). When some thermoplastics are heated above their glass transition temperature, they move from a "glassy" state to a softer, rubber like state. Some thermoplastics, such as, poly(lactic acid) (PLA)[167–170] or thermoplastic polyurethanes[171–174] have fairly high glass-transition temperatures between 45 and 60°C, so they exist in their "glassy" state at room temperature and undergo stiffness change after being Joule heated through T_g alone. However, other semicrystalline polymers, such as polycaprolactone (PCL),[175–178] have much lower glass transition temperatures (–60 °C), and exist in their rubber-like state (above T_g) at room temperature. Thus, materials like PCL must be Joule heated above their melting temperature (T_m = 60 °C for PCL) to undergo stiffness change, as heating through T_g does not allow for viscous flow. Figure 7A displays examples of this electrothermal softening.

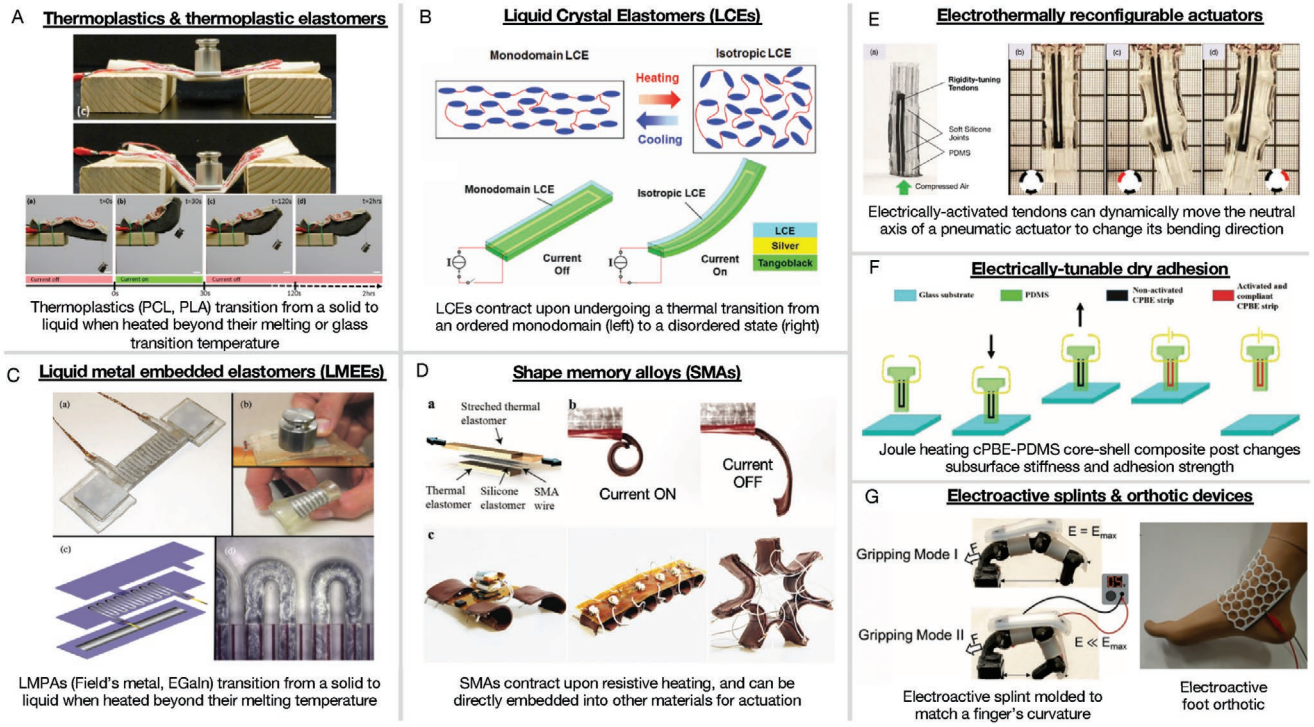

Figure 7. Electrothermal materials. A) Joule heating a sheet with variable stiffness fibers to reduce its stiffness (upper), Joule heating to lock in different curvatures of a soft robotic arm (lower). B) Schematic of LCE operation and the resulting stiffness change via geometric alteration. C) Stiffness change of an LMEE via Joule heating of a low-melting point alloy arranged in serpentine traces. D) Schematic of SMA operation and the resulting stiffness change via electrically driven length contraction (upper). SMAs have been embedded within the structure of locomotive robots for actuation. E) Reconfigurable pneumatic finger actuators via Joule-heated cTPE tendons. F) Adhesive gripper with electrically programmed stiffness via Joule heating of a cPBE core. G) Electroactive splint with programmable stiffness via Joule heating of a cTPE matrix to block finger motion (left), and via Joule heating of a PLA matrix to block ankle motion. A) Reproduced with permission.[168] Copyright 2016, IEEE. B) Reproduced with permission.[199] Copyright 2017, Royal Society of Chemistry. C) Reproduced with permission.[188] Copyright 2013, IOP Publishing. D) Reproduced with permission.[218] Copyright 2019, Wiley-VCH. E) Reproduced with permission.[29] Copyright 2015, IOP Publishing. F) Reproduced with permission.[180] Copyright 2018, Wiley-VCH. G) Left part: Reproduced with permission.[219] Copyright 2017, Wiley-VCH. Right part: Reproduced under the terms of the CC-BY Creative Commons Attribution 4.0 International license (https://creativecommons/licenses/by/4.0).[169] Copyright 2018, IEEE.

A TPE is a soft material that has a thermoplastic polymer embedded within its interior.[166] Thermoplastics, on their own, soften as they are heated above T_g and then T_m, but if they are deformed in this "soft" state, they do not recover their original shape simply through cooling. Therefore, thermoplastics have been combined with an elastomer matrix to allow for softening with heating and shape recovery upon subsequent cooling. For most thermoplastic-based electrothermal materials that undergo stiffness change via Joule heating, embedded heaters such as conductive wires (often Nichrome or Ni–Ti),[167,177] or graphene elements[169,170] are used to generate heat. However, the recent development of conductive TPEs has removed the requirement for external Joule heating elements. For example, Shan et al. introduced an electrothermal stiffness change material comprised of a conductive propylene-based elastomer (cPBE) embedded in an elastomeric sheet of PDMS.[29] By integrating a percolating network of conductive carbon black into a polypropylene-ethylene thermoplastic, an electric current can be directly applied to the cPBE composite to induce stiffness changes without any external heating elements. Thus, conductive TPEs reduce the number of components in any given design, making them compatible with many actuation or adhesion systems.[179,180]

The stiffness change of a shape memory polymer (SMP) is also governed by a glass or melting transition upon electrical heating. SMPs are typically composed of two polymeric materials: an elastic segment, whose stiffness is always constant, and a transition segment, whose stiffness can be reduced by the introduction of an outside stimulus, such as, heat, via some external source, such as, a Joule heater.[181] After heat is applied, the transition segment moves through its T_g or T_m, and the stiffness of the SMP drops. The SMP can then be deformed by an external load to reach a new shape, which can be locked-in by rapid cooling and the subsequent stiffening of the transition segment. When heat is re-applied, the transition segment softens once again, and the deformed elastic segment provides a restoring force to move the SMP back to its original shape.[181] If the application of heat and an external load are required to trigger the initial shape change, then heat alone must trigger shape recovery to classify that material as an SMP. Examples of SMPs include glassy thermosets such as polynorbornene, chemically crosslinked semicrystalline rubbers such as PCL, rubbery, epoxy-based materials, and physically crosslinked blocked copolymers.[182–184]

4.2.2. Liquid-Metal-Embedded Elastomers

When a network of liquid metal (LM) or low-melting-point alloy (LMPA) is dispersed in a elastomeric matrix, it is known as a LMEE.[39] Since LMPAs have low melting temperatures (T_m = 62 °C for Field's metal, an alloy of indium, tin, and bismuth), high elastic moduli at room temperature, and higher thermal conductivities than many polymers, they are an attractive material to realize electrothermal stiffness change via Joule heating.[30,185] Furthermore, elastomers utilized in LMEEs, such as, silicone rubber, are thermally stable through the melting transition temperature of LMPAs, and can sustain high strains when the LMPA is Joule heated. Notably, LMEEs comprised of polysiloxane and eutectic gallium–indium droplets can achieve up to 600% strain without failure, and LMEEs with randomly dispersed networks of liquid metal can sustain strains up to 125% without changes in electrical resistance, due to the liquid metal's ability to stretch with the surrounding elastomer.[39] Therefore, additional power is not required to Joule heat an LMEE which has been deformed by such an amount. While there are numerous examples of LMEEs composed of LMPAs (typically arranged in serpentine traces, as shown in Figure 7C) embedded directly into PDMS or silicone matrices that undergo stiffness changes via Joule heating,[186–189] they can also be formed into fibers with programmable stiffness.[185,190]

4.2.3. Shape Memory Alloys

SMAs are materials whose shape and stiffness can be programmed through thermally induced phase transitions. Common SMAs, such as, Ni–Ti (Nitinol), are governed by a reversible martensitic-austenite transition.[191] In a typical example, the Ni–Ti SMA is annealed at high temperature and cooled, which sets its martensitic state and an initial, "remembered" shape. At this point, the SMA is malleable ($E \approx$ 28–41 GPa) and can be mechanically deformed into a new shape. After heating the material to an austenite state, the SMA returns to the original shape, which it retains after cooling and becomes stiff ($E \approx$ 82–100 GPa). A comprehensive review of robotic SMA applications can be found in Huang et al.[192] In particular, SMAs used for shape and stiffness change are common in reconfigurable structures, jointed locomotive robots, and wearable skins.[193–195]

4.2.4. Liquid Crystal Elastomers

Another type of electrothermal material whose stiffness and shape can be actively programmed is a LCE. An LCE is comprised of rigid molecules, mesogens, in a chemically crosslinked polymer network separated by flexible spacers. The shape and stiffness of an LCE can be controlled by changing the mesogen order using a thermal stimulus, such as, Joule heating, similar to an SMA. LCEs exhibit larger mechanical strains in their heated, softened state (from 50% to 400%) compared to SMAs (4–8%), and lower Young's moduli (E < 10 MPa).[192,196] To control the shape and stiffness of an LCE, the mesogens must be macroscopically aligned to form an anisotropic monodomain, which is typically done by mechanically straining a partially crosslinked network. After alignment, the material is allowed to fully crosslink in the fixed director orientation.[197] This "two-step" crosslinking process was developed by Küpfer and Finkelmann and is still used today to change the director orientation of LCEs.[198] Upon heating the material past its nematic–isotropic transition temperature (T_i), the mesogen alignment is removed, causing the LCE to enter an isotropic, disordered state, where it contracts.[199] In order to Joule heat the material, researchers have integrated surface heaters[199–205] or conductive fillers such as carbon black,[206,207] carbon nanotubes,[208,209] and liquid metal emulsions[210,211] into LCE networks to render them electrically conductive. The conductive fillers have a large impact on the maximum actuation strain (and stiffness change) of the LCE, which will be discussed in Section 4.2.6. Finally, while Joule heating is the most common method used to trigger the nematic-isotropic transition of an LCE, the same can be achieved using a very large electric field (10^6 Vm^{-1}), whose introduction or removal can change the director alignment.[212,213] Joule heating is, however, the most common stimulus for triggering stiffness change in an LCE and can be done at reduced voltages (<30 V).

4.2.5. Thermoresponsive Hydrogels

A thermoresponsive hydrogel is a hydrophilic network of polymer chains dispersed in water which changes shape and stiffness upon heating or cooling through a critical solution temperature that dictates the hydrophobic and hydrophilic interactions between polymer chains.[214–216] For example, poly(*N*-isopropylacrylamide), or PNIPAm, a common type of negative thermoresponsive hydrogel, has a lower critical solution temperature (LCST) of 32 °C. Below its LCST, PNIPAm exhibits hydrophilic behavior, as hydrogen bonds can form between the polymer chains and water molecules. When heated above its LCST, PNIPAm exhibits hydrophobicity, as those hydrogen bonds break, and the water molecules are expelled from the polymer network, causing contraction. By changing the monomer composition of the gel, the LCST can be adjusted typically through copolymerization with another hydrophilic or hydrophobic monomer.[216] Similar to TPEs and LCEs, adding a percolating network of conductive carbon nanofibers into the gel network can enable Joule heating and autonomous actuation of the gel without immersion in a temperature-controlled liquid.[217]

4.2.6. Implementations

Joule heating allows for the selective programming of material stiffness within the bulk of a structure via the placement of conductive elements, which has made electrothermal materials attractive in reconfigurable actuators, wearable skins, and grippers with switchable adhesion. Canonical soft robotic bending actuators are comprised of an elastomeric balloon body with an internal cavity that can be inflated using a pressurized pneumatic fluid. On one side of any soft balloon actuator, there is an inextensible material (typically a stiff elastomer or fabric). When an internal soft cavity is pressurized, the actuator expands,

bending away from the inextensible material.[44] By arranging electrothermal, programmable stiffness elements in different locations on a externally driven actuator (e.g., pneumatic, motor-driven), researchers have developed bending actuators whose inextensible and extensible regions can be shifted in real time, thus enabling real-time control of bending direction. For these devices, the electrothermal elements provide stiffness change, while an external input triggers shape change. For example, Shan et al. demonstrated a pneumatic finger with integrated cPBE tendons that softened from 37 to 1.5 MPa in ≈6 s upon Joule heating with an input voltage of 150 V and consumed 3.3 W of power. Upon softening, the neutral axis of the finger was shifted in real time using specific tendons that are electrically activated.[29] Researchers have developed a variety of bending actuators with adjustable joints using different electrothermal materials. For example, Zheng et al. used electrical current to heat Field's metal within a pneumatic balloon actuator, which enabled control of its bending direction upon inflation.[187] Others have used thermoplastic polyurethane-based SMPs and Joule heating to achieve grippers with adjustable joints.[171–173] Likewise, Shintake et al. demonstrated a DE-based actuator whose bending direction was actively changed by electrically heating an integrated LMPA element.[189] By decoupling stiffness change and shape change, actuators with electrothermal, programmable stiffness can provide large strains and high output forces at the expense of complex designs with many components that must be carefully integrated together for functionality. Researchers have also deployed electrothermal actuators to directly cause shape and stiffness change without any external input. SMA wires, which can be electrically activated using an applied current, are commonly used for the actuation of robotic hinges, and are directly placed on a rigid fold pattern,[193,220–222] the surface of a soft polymer, or within the bulk of a soft polymer.[195,218,223–227] Robotic hinges driven by SMAs have been used in robots capable of gaited locomotion and structural self-assembly, but can only achieve small strains (4–8%) and small degrees of stiffness change, which limits their use.[227] Joule heated LCEs have also recently become attractive candidates for robotic actuators, as demonstrated in LCE-based soft grippers and untethered soft crawlers.[202,205] LCEs can achieve larger strains than SMAs, but lack the speed and energy efficiency of other materials with electroprogrammable stiffness that directly couple shape and stiffness change, such as DEs and electrohydraulics.[205] However, despite energy losses from Joule heating, LCEs only need low voltages for actuation, and, as a result, are more desirable for untethered systems where small, lightweight, commercially available power sources are attractive.

Electrothermal materials have spurred the development of novel wearable skins and fabrics for medical applications, particularly orthotic splints for active joint immobilization. For example, Rich et al. demonstrated a conductive thermoplastic elastomer (cTPE) splint with liquid metal electrodes, whose axial stiffness was reduced from 10 to 1 MPa in 40 s when Joule heated with a 5 V input, consuming 5 W of power.[219] When heated, the splint was molded to fit a patient's hand, and provided rigid mechanical support after cooling. The splint needed to be lined with nylon fabric to protect the user from burns. By using liquid metal electrodes, the entire cTPE matrix was melted and fabricated into different complex shapes that underwent the full stiffness transition. Similarly, Taghavi et al. developed a wearable foot-drop orthotic device based on the electrothermal stiffness change of PLA with embedded conductive graphene.[169] This device conformed to the shape of a patient's ankle in the soft state, and then helped maintain a foot angle in the rigid state, which was critical for walking and general mobility. Since the stiffness of this orthotic was easily programmed with an electric current, a user could soften the device for added comfort in scenarios where the orthotic was not required. Fabrics and fibers with electroprogrammable stiffness via Joule heating can also be added to inanimate soft structures to induce a desired motion or force output. For example, Tonazzini et al. demonstrated a LMPA-based fiber whose stiffness was programmed between 887.8 and 1.2 MPa in as little as 29 s using an applied current of 1.1 A.[185] By weaving the programmable stiffness fiber into a cotton fabric, it was formed into a wearable cast for bone injuries that exhibited improved speed and breathability compared to current synthetic cast materials. Such a fiber could also be molded into an arbitrary soft end-effector for added protection and strength upon large external impacts or during actuation events that require high force outputs.[185] Finally, Yuen et al. demonstrated another programmable stiffness fiber with a thermoplastic core that could soften upon Joule heating with integrated SMA wires.[168] By sewing the fibers into a cotton fabric, the researchers created a programmable fabric that could be applied to a foam block to simulate a soft robotic arm. After actuating the fibers, the fabric enabled the foam block to bend and lift a mass. To improve fabrics with electroprogrammable stiffness, the weaving pattern of Joule-heated fibers within a fabric can be optimized for enhanced force capacities and response times.

Furthermore, new approaches to automate surgery have employed SMA springs for actuation. For example, Alcaide et al. and Seok et al. demonstrated biomimetic meshworm robots which utilized Joule heating to activate SMA springs, producing a crawling gait for peristaltic locomotion in an endoscopic setting.[228,229] Similarly, Kim et al. developed a SMA-driven intercranial robot for tumor resection.[230] In all, electrothermal materials whose stiffness can be programmed via changes in geometry are promising tools for minimally invasive surgery due to their large energy densities per cycle, but they suffer from slow cycle frequencies due to long cooling times.[229]

Electrothermal materials with programmable stiffness have also been exploited to realize systems with switchable dry adhesion. For example, Tatari et al. demonstrated a composite core-shell post with an integrated cPBE core whose stiffness could be switched between 175 and 1 MPa upon Joule heating for adhesive gripping, while consuming ≈2 W of power, as shown in Figure 7F.[180] In the rigid state, the post had a stiff core and a compliant shell, which led to high adhesion strength between the gripper and contact surface. When the cPBE was activated with an applied voltage, it softened, changing the stress distribution at the contact interface. This electrically driven change drove delamination and led to a factor of 6 reduction in adhesion strength. Similarly, Eisenhaure and Kim developed an SMP doped with carbon black, which allowed for tunable adhesion via Joule heating.[183] While this work presented another option for tunable dry adhesion via Joule heating and stiffness

programming, other electrothermal materials have been implemented for adhesion control, albeit without electrically controlled heaters. For example, the surface topology of SMPs can be changed via heat,[231] and Wang et al. implemented external heating to introduce specific wrinkling patterns into an SMP on a PDMS substrate, which then displayed programmable and reversible adhesion to a substrate.[232] Likewise, Lee et al. developed a PNIPAm hydrogel whose swelling behavior could be controlled via thermal stimulation in an octopus-inspired gripper,[233] and Krahn et al. presented a pillar-based switchable adhesive based on the melting transition of wax contained in PDMS cavities.[234,235] Finally, Ye et al. demonstrated a material system capable of switchable adhesion that relied on the thermal stiffness modulation of a gallium (Ga) liquid metal layer.[236] In this work, the researchers coated the tip of a heated elastomeric post with a liquid Ga drop that was covered in a layer of gallium oxide. The heated post was then brought into contact with the substrate (so the Ga stays in its liquid state) and cooled, leading to high-adhesion. When the post was heated once more, the Ga layer liquefied, allowing for object release. Future switchable adhesives, comprised of a variety of thermally activated materials, could employ approaches similar to that of Tatari et al. and Eisenhaure et al. for integrated Joule heating, which used conductive wires and conductive fillers for internal heat generation.[180,183]

While all of these systems show promise, they all require a user-in-the-loop to manually program the temperature of different electrothermal stiffness elements. To solve this issue, McEvoy et al. introduced a electrothermal material system with programmable shape and stiffness that integrated actuation, control, communication, and computation in one package.[175–178] Each programmable stiffness element utilized embedded nichrome heaters to melt a thermoplastic PCL layer encased in siloxane rubber. This system could soften from an elastic modulus of 200 to 2 MPa in 200 s using a 12 V input signal. By assembling a number of PCL-based programmable stiffness elements in series, different cells could be heated and cooled in real time to form and lock-in different curvatures. By integrating thermistors and a microcontroller into the material system, the actuator autonomously deformed to a specific curvature based on a programmed stiffness profile. While Joule heating of each programmable stiffness element occurred in approximately 3 min, convective cooling of the PCL occurred in 25 min.[176] This significant difference in heating and cooling times precludes the use of electrothermal materials in applications which require fast stiffening and softening cycles, such as pick-and-place robotic grasping.[180] Future work should focus on the reduction of both heating and cooling times, and the integration of novel flexible sensors into the programmable stiffness material to monitor temperature, stiffness, and strain while minimizing the number of components needed for full functionality.[43,237–240]

4.2.7. Materials

Different material properties inherent to electrothermal materials and Joule heating have significant effects on the magnitude and the speed of programmable stiffness change. Nichrome, gold, and nitinol wires have all been employed as resistive heaters to trigger a phase transition, but are subject to a few major problems. First, since conductive heating is dependent on wire geometry, small geometric defects can lead to local hot and cold locations on any one surface heating element.[168] As a result, surface heaters may not lead to the uniform stiffness changes throughout the bulk of a material, which is undesirable for many applications, especially those where specific stiffnesses must be programmed for precise curvature control. Next, conductive heating at extremely high transition temperatures can permanently damage surface heating elements, leading to failure or delamination from the phase-change material after cyclical operation.[202] Furthermore, surface heating elements can restrict the deformation of the material system, and their ability to heat is limited by the intrinsic thermal conductivity of the phase-change material. For example, for LCEs, whose stiffness change is directly coupled to shape change, surface heaters can only trigger a nematic to isotropic phase transition for specimens with thicknesses on the order of hundreds of micrometers.[210] Surface heaters, however, can drive a meaningful, geometrically driven stiffness change in an electrothermal material by triggering a liquid–vapor transition in an elastomeric matrix innervated with liquid ethanol.[241] This material system can achieve a 140% volumetric expansion in one direction upon Joule heating with a nichrome surface heater, but is limited by slow heating/cooling times and degradation due to ethanol evaporation. Lastly, the total degree of stiffness change and the time required to Joule heat and soften an electrothermal material is dependent on the type of phase-change material. By using a phase-change material with a lower transition temperature, the time required for Joule heating and softening can be reduced. Likewise, by applying larger voltages, the softening time can also be reduced, as the electrical power rises with the square of the applied voltage.[219] The passive cooling of any electrothermal material is limited by convection and conduction, which prevents rapid stiffening after the removal of an electrical input, although the amount of cooling required to re-stiffen will depend on the material's T_g or T_m. To reduce cooling times, passive cooling systems can be replaced with active ones, such as Peltier junctions or liquid-flow channels, although these solutions require additional electrical power, complicate manufacturing, and add both size and weight.[241] Through 3D printing, electrothermal phase-change materials can be arranged into metamaterial architectures with reduced feature sizes. Since the time required for stiffness change via Joule heating decreases with feature size, additive manufacturing of optimized internal geometries is a promising approach to realize faster heating/cooling and thus, reduced stiffening/de-stiffening times.[201,242]

To mitigate a number of these issues, surface heaters can be replaced with conductive fillers that can be embedded directly in the programmable material for direct Joule heating. A few examples of such fillers include carbon black and carbon nanotubes. These fillers alleviate the need for surface heaters for programmable stiffness change. Furthermore, fillers can increase the thermal conductivity of the material system, which can shorten passive cooling times.[241] Despite these advantages, they dramatically restrict the deformation of the resulting material. Agrawal et al. demonstrates that this effect is especially

apparent in LCEs. When an LCE is combined with 15% carbon black (by weight), its actuation strain is reduced from 35% (without any fillers) to 5.2% with the added filler.[207] To mitigate this issue, researchers have implemented internal liquid metal elements for Joule heating. Since liquid metals can flow with the elastomer in their soft state, they do not prevent the phase-change material from deforming when stretched.[188,210,211] Liquid metal traces can be specifically arranged into serpentine patterns to enhance actuation strains,[188,200] and liquid metal particles can be sized or shaped to control the stiffness and shape change of an LMEE or LCE.[211,243] Unfortunately, liquid metal heating elements or fillers usually need to be completely sealed from the phase-change material, which adds fabrication complexity and sources of heat dissipation to the system.[188] Liquid metals can also serve as electrodes for an electrothermal material with an added conductive filler, like the cTPE presented by Rich and coworkers.[219] By arranging LM electrodes across the entire face of the cTPE, the effective resistance of the system can be reduced. Thus, the minimum required voltage to trigger melting and stiffness change for a cTPE can be reduced from 150 to 5 V, and the minimum required time for activation can be reduced from 6 to 2 s.[29,219] Despite this improvement, it is notable that the addition of conductive fillers can increase the heat capacity of an electrothermal material. This leads to an increase in the total amount of heat required to reach a critical transition temperature and trigger a stiffness change, which may be a disadvantage for some applications. Liquid metals and low-melting point alloys have also been successfully integrated into hydrogel and porous foam networks for thermally driven, programmable stiffness and shape change.[30,244] Nevertheless, some liquid metals, including mercury, are toxic and cannot be safely implemented in LMEEs that contact human tissues.[245] However, common LMPAs including Field's metal and Galistan are nontoxic, and have been safely used in biomedical applications.[246] Overall, materials with electroprogrammable stiffness triggered by Joule heating are advantageous compared to programmable materials triggered by external heating for untethered applications and selective areal programming, as surface heaters and fillers can be more easily directed to specific locations within a material system to produce targeted stiffness changes.

5. Conclusion and Outlook

We have presented a comprehensive overview of materials that allow stiffness to be modulated via electrical activation. These materials exploit either electrostatics or phase-change to modulate stiffness, and the combination of material properties, material processing, and material design play a critical role in improving performance. There are several opportunities for further progress in the field of materials with electroprogrammable stiffness. First, for electroadhesives, activation voltages could be significantly reduced and changes in stiffness could be increased via the development of ionoelastomer materials with ionic double layers that transmit electrostatic forces over nanometer length scales,[74] or the use of Johnsen–Rahbek electroadhesives with semiconductive dielectric layers of resistivities less than 10^{10} Ω cm.[48] Furthermore, electroadhesives should be modeled as adhered surfaces, whose in-plane electrode shapes and stiffnesses can be specifically controlled to inhibit crack formation, thus increasing force capacities while decreasing electrode areas and driving voltages.[75,247] New geometric architectures for electrorheological material systems with reduced viscosity could increase dielectric particle chain formation, which, in turn, would increase changes in shear stiffness. Similarly, novel geometric architectures and manufacturing techniques for electrohydraulic materials could enable smaller gaps between compliant electrode layers that increase blocking forces. Electrohydraulic material systems would also benefit from the use of higher permittivity dielectric liquids in place of oil-based mediums frequently used today. Water-based dielectric liquids could enable materials that undergo larger changes in shape and stiffness, but the challenge of large electric field generation without short circuits or electrolysis must be solved to realize this goal.

For electrochemical materials, activation and de-activation times can be decreased by implementing materials with reduced ion and electron transport resistances, for example, by reducing material thicknesses to the micrometer or nanometer scale or improving conductivity and diffusivity in the bulk materials. This, in turn, can increase the rate of redox reactions at the core of electrochemically driven stiffness programming. Future improvements to electrochemically driven microlattices can derive inspiration from materials studied in battery literature that show large degrees of volumetric expansion, but can also be cycled hundreds of times without failure by protecting the electrode surface and decreasing the lattice size.[157,248] The activation and de-activation times of electrothermal materials can be reduced by using electrode materials with greater thermal conductivities and higher heat transfer rates to their environments. Such advances could enable rapid Joule heating and subsequent cooling without compromising their large stiffness change and material deformability.

There are also clear opportunities for combined approaches. Material systems can be designed to leverage electrostatics and phase-changes concurrently to optimize stiffness modulation or activation times, leveraging the strengths of both strategies. The next-generation of electrically tunable materials should also be fully reversible and exhibit compatibility with a variety of electrical inputs for stiffness programming, as different applications may require different triggers that change in time.[249] Two clear challenges for electroprogrammable materials that are compatible with multiple stiffness programming inputs are fabrication and integration, as separate stiffness-tuning mechanisms will have to be codesigned within the bulk of one material. New analytical models of electroprogrammable materials allow for improved designs in emerging applications, although new modeling techniques, including computational models, will be required as these materials become more complex.[250] Advances in additive manufacturing, such as 4D printing and multimaterial printing, provide exciting avenues for electroprogrammable materials, as they enable the creation of complex geometries and composites comprised of stimuli-responsive materials that could not be previously realized by traditional, multistep manufacturing approaches.[251,252]

As development in materials science, electrochemistry, physics, electrical engineering, mechanical engineering, and robotics

continues to progress into the future, we foresee new materials with electroprogrammable stiffness that exhibit increased stiffness modulation ranges, decreased operating voltages, and decreased activation/deactivation times. As a result, these materials will be integral to a new wave of nascent technologies. Electroprogrammable materials for haptic devices could integrate with human–machine interfaces and dynamically change their shape and stiffness to realistically simulate the characteristics of real objects in a virtual setting. Electrically activated fabrics could enable wearable medical technologies, such as splints, that could change their shape and stiffness to match the body shape of a user. Lightweight electroprogrammable skins could be inexpensively applied to soft robotic manipulators to help them carry larger payloads in exploration scenarios without risking damage to their local environment. In all, emergent materials with electroprogrammable stiffness are the building blocks for autonomous, "smart" structural components for machines and robots that can decide to modulate their stiffness in response to changes in their environment. However, to realize materials with true autonomy, there are also complimentary needs for critical advancements in sensory networks, power sources, and feedback control systems. Such subsystems will have to be cleverly integrated with materials with electroprogrammable stiffness in the next-generation of multifunctional robots and machines, whose designs more closely resemble those of biological organisms.

Acknowledgements

D.J.L. was partially supported by a Department of Education GAANN fellowship grant number P200A160282 to the Department of Mechanical Engineering and Applied Mechanics at the University of Pennsylvania. D.J.L. and K.T.T. acknowledge support from the National Science Foundation Robotics Initiative, award #1830475. D.J.L. and J.H.P. were also partially supported by the National Science Foundation Emerging Frontiers in Research and Innovation (EFRI) award #1935294.

Conflict of Interest

The authors declare no conflict of interest.

Keywords

actuators, electroprogrammable stiffness, programmable materials, robotics, stiffness control, tunable modulus, tunable stiffness

Received: November 23, 2020
Revised: February 19, 2021
Published online: July 9, 2021

[1] P. Polygerinos, N. Correll, S. A. Morin, B. Mosadegh, C. D. Onal, K. Petersen, M. Cianchetti, M. T. Tolley, R. F. Shepherd, *Adv. Eng. Mater.* **2017**, *19*, 1700016.
[2] S. S. Robinson, C. A. Aubin, T. J. Wallin, S. Gharaie, P. A. Xu, K. Wang, S. N. Dunham, B. Mosadegh, R. F. Shepherd, *Adv. Mater. Technol.* **2018**, *3*, 1800233.
[3] B. C. M. Murray, X. An, S. S. Robinson, I. M. van Meerbeek, K. W. O'Brien, H. Zhao, R. F. Shepherd, *Adv. Mater.* **2015**, *27*, 6334.
[4] T. Moriga, N. Aoyama, K. Tanaka, *Polym. J.* **2015**, *47*, 400.
[5] Y. Wang, M. A. Minor, *IEEE/ASME Trans. Mechatronics.* **2018**, *23*, 2974.
[6] D. W. Haldane, M. M. Plecnik, J. K. Yim, R. S. Fearing, *Sci. Rob.* **2016**, *1*, eaag2048.
[7] J. H. Pikul, S. Li, H. Bai, R. T. Hanlon, I. Cohen, R. F. Shepherd, *Science* **2017**, *358*, 210.
[8] S. R. Hamner, A. Seth, S. L. Delp, *J. Biomech.* **2010**, *43*, 2709.
[9] F. J. Valero-Cuevas, *J. Biomech.* **2005**, *38*, 673.
[10] D. Lentink, U. K. Müller, E. J. Stamhuis, R. de Kat, W. van Gestel, L. L. M. Veldhuis, P. Henningsson, A. Hedenström, J. J. Videler, J. L. van Leeuwen, *Nature* **2007**, *446*, 1082.
[11] J. F. Wilson, U. Mahajan, S. A. Wainwright, L. J. Croner, *J. Biomech. Eng.* **1991**, *113*, 79.
[12] C. Laschi, M. Cianchetti, B. Mazzolai, L. Margheri, M. Follador, P. Dario, *Adv. Robot.* **2012**, *26*, 709.
[13] H. E. Huxley, *Science* **1969**, *164*, 1356.
[14] I. W. Hunter, S. Lafontaine, in *Tech. Dig. IEEE Solid-State Sensor and Actuator Workshop*, IEEE, Piscataway, NJ, USA **1992**, pp. 178–185; https://doi.org/10.1109/SOLSEN.1992.228297.
[15] J. R. Capadona, K. Shanmuganathan, D. J. Tyler, S. J. Rowan, C. Weder, *Science* **2008**, *319*, 1370.
[16] M. H. Dickinson, C. T. Farley, R. J. Full, M. A. R. Koehl, R. Kram, S. Lehman, *Science* **2000**, *288*, 100.
[17] P. Polygerinos, Z. Wang, K. C. Galloway, R. J. Wood, C. J. Walsh, *Rob. Auton. Syst.* **2015**, *73*, 135.
[18] H. Zhao, J. Jalving, R. Huang, R. Knepper, A. Ruina, R. Shepherd, *IEEE Rob. Autom. Mag.* **2016**, *23*, 55.
[19] J. Shintake, V. Cacucciolo, D. Floreano, H. Shea, *Adv. Mater.* **2018**, *30*, 1707035.
[20] R. Hinchet, H. Shea, *Adv. Mater. Technol.* **2020**, *5*, 1900895.
[21] V. Ramachandran, J. Shintake, D. Floreano, *Adv. Mater. Technol.* **2019**, *4*, 1800313.
[22] A. Ramezani, S.-J. Chung, S. Hutchinson, *Sci. Rob.* **2017**, *2*, eaal2505.
[23] E. Chang, L. Y. Matloff, A. K. Stowers, D. Lentink, *Sci. Rob.* **2020**, *5*, eaay1246.
[24] B. Mosadegh, P. Polygerinos, C. Keplinger, S. Wennstedt, R. F. Shepherd, U. Gupta, J. Shim, K. Bertoldi, C. J. Walsh, G. M. Whitesides, *Adv. Funct. Mater.* **2014**, *24*, 2163.
[25] H. Yuk, S. Lin, C. Ma, M. Takaffoli, N. X. Fang, X. Zhao, *Nat. Commun.* **2017**, *8*, 14230.
[26] E. Brown, N. Rodenberg, J. Amend, A. Mozeika, E. Steltz, M. R. Zakin, H. Lipson, H. M. Jaeger, *Proc. Natl. Acad. Sci. USA* **2010**, *107*, 18809.
[27] Y. S. Narang, J. J. Vlassak, R. D. Howe, *Adv. Funct. Mater.* **2018**, *28*, 1707136.
[28] K. W. O'Brien, P. A. Xu, D. J. Levine, C. A. Aubin, H.-J. Yang, M. F. Xiao, L. W. Wiesner, R. F. Shepherd, *Sci. Rob.* **2018**, *3*, eaau5543.
[29] W. Shan, S. Diller, A. Tutcuoglu, C. Majidi, *Smart Mater. Struct.* **2015**, *24*, 065001.
[30] I. M. V. Meerbeek, B. C. M. Murray, J. W. Kim, S. S. Robinson, P. X. Zou, M. N. Silberstein, R. F. Shepherd, *Adv. Mater.* **2016**, *28*, 2801.
[31] R. V. Beblo, L. M. Weiland, *J. Appl. Mech.* **2009**, *76*, 011008.
[32] P. Testa, R. W. Style, J. Cui, C. Donnelly, E. Borisova, P. M. Derlet, E. R. Dufresne, L. J. Heyderman, *Adv. Mater.* **2019**, *31*, 1900561.
[33] J. A. Jackson, M. C. Messner, N. A. Dudukovic, W. L. Smith, L. Bekker, B. Moran, A. M. Golobic, A. J. Pascall, E. B. Duoss, K. J. Loh, C. M. Spadaccini, *Sci. Adv.* **2018**, *4*, eaau6419.
[34] D. Rus, M. T. Tolley, *Nature* **2015**, *521*, 467.
[35] M. Manti, V. Cacucciolo, M. Cianchetti, *IEEE Rob. Autom. Mag.* **2016**, *23*, 93.
[36] L. Wang, Y. Yang, Y. Chen, C. Majidi, F. Iida, E. Askounis, Q. Pei, *Mater. Today* **2018**, *21*, 563.
[37] J. M. McCracken, B. R. Donovan, T. J. White, *Adv. Mater.* **2020**, *32*, 1906564.

[38] A. B. Croll, N. Hosseini, M. D. Bartlett, *Adv. Mater. Technol.* **2019**, *4*, 1900193.
[39] N. Kazem, T. Hellebrekers, C. Majidi, *Adv. Mater.* **2017**, *29*, 1605985.
[40] A. O'Halloran, F. O'Malley, P. McHugh, *J. Appl. Phys.* **2008**, *104*, 071101.
[41] Y. Qiu, E. Zhang, R. Plamthottam, Q. Pei, *Acc. Chem. Res.* **2019**, *52*, 316.
[42] B. Jenett, S. Calisch, D. Cellucci, N. Cramer, N. Gershenfeld, S. Swei, K. C. Cheung, *Soft Rob.* **2017**, *4*, 33.
[43] H. Zhao, K. O'Brien, S. Li, R. F. Shepherd, *Sci. Rob.* **2016**, *1*, eaai7529.
[44] F. Ilievski, A. D. Mazzeo, R. F. Shepherd, X. Chen, G. M. Whitesides, *Angew. Chem.* **2011**, *123*, 1930.
[45] J. R. Amend, E. Brown, N. Rodenberg, H. M. Jaeger, H. Lipson, *IEEE Trans. Rob.* **2012**, *28*, 341.
[46] A. Johnsen, K. Rahbek, *J. Inst. Electr. Eng.* **1923**, *61*, 713.
[47] J. Guo, J. Leng, J. Rossiter, *IEEE Trans. Rob.* **2019**, *36*, 313.
[48] S. Qin, A. McTeer, *J. Appl. Phys.* **2007**, *102*, 064901.
[49] B. N. J. Persson, *J. Chem. Phys.* **2018**, *148*, 144701.
[50] M. R. Sogard, A. R. Mikkelson, M. Nataraju, K. T. Turner, R. L. Engelstad, *J. Vac. Sci. Technol., B: Microelectron. Nanometer Struct.–Process., Meas., Phenom.* **2007**, *25*, 2155.
[51] S. B. Diller, S. H. Collins, C. Majidi, *J. Intell. Mater. Syst. Struct.* **2018**, *29*, 3804.
[52] H. Imamura, K. Kadooka, M. Taya, *Soft Matter* **2017**, *13*, 3440.
[53] S. H. Collins, M. B. Wiggin, G. S. Sawicki, *Nature* **2015**, *522*, 212.
[54] S. Diller, C. Majidi, S. H. Collins, in *2016 IEEE Int. Conf. on Robotics and Automation (ICRA)*, IEEE, Piscataway, NJ, USA **2016**, pp. 682–689.
[55] A. S. Chen, S. Bergbreiter, *Smart Mater. Struct.* **2017**, *26*, 025028.
[56] R. Hinchet, V. Vechev, H. Shea, O. Hilliges, in *Proc. 31st Annu. ACM Symp. on User Interface Software and Technology - UIST '18*, ACM Press, **2018**, pp. 901–912.
[57] D. M. Aukes, B. Heyneman, J. Ulmen, H. Stuart, M. R. Cutkosky, S. Kim, P. Garcia, A. Edsinger, *Int. J. Rob. Res.* **2014**, *33*, 721.
[58] M. E. Karagozler, J. D. Campbell, G. K. Fedder, S. C. Goldstein, M. P. Weller, B. W. Yoon, in *2007 IEEE/RSJ Int. Conf. on Intelligent Robots and Systems (IROS)*, IEEE, Piscataway, NJ, USA **2007**, pp. 2779–2786.
[59] F. Previtali, T. Delpero, A. Bergamini, A. F. Arrieta, P. Ermanni, *Extreme Mech. Lett.* **2015**, *3*, 82.
[60] W. Raither, E. Furger, M. Zündel, A. Bergamini, P. Ermanni, *J. Intell. Mater. Syst. Struct.* **2015**, *26*, 1609.
[61] A. Bergamini, R. Christen, B. Maag, M. Motavalli, *Smart Mater. Struct.* **2006**, *15*, 678.
[62] A. Bergamini, R. Christen, M. Motavalli, *Smart Mater. Struct.* **2007**, *16*, 575.
[63] L. Di Lillo, W. Raither, A. Bergamini, M. Zündel, P. Ermanni, *Appl. Phys. Lett.* **2013**, *102*, 224106.
[64] T. Wang, J. Zhang, Y. Li, J. Hong, M. Y. Wang, *IEEE/ASME Trans. Mechatronics* **2019**, *24*, 424.
[65] O. Tabata, S. Konishi, P. Cusin, Y. Ito, F. Kawai, S. Hirai, S. Kawamura, *Sens. Actuators, A* **2001**, *89*, 119.
[66] M. Taghavi, T. Helps, J. Rossiter, *Sci. Rob.* **2018**, *3*, eaau9795.
[67] P. Jain, E. J. Rymaszewski, *IEEE Trans. Adv. Packag.* **2002**, *25*, 454.
[68] B. Li, Y.-P. Cao, X.-Q. Feng, H. Gao, *Soft Matter* **2012**, *8*, 5728.
[69] J. Guo, T. Bamber, M. Chamberlain, L. Justham, M. Jackson, *J. Phys. D: Appl. Phys.* **2016**, *49*, 415304.
[70] C. Cao, X. Gao, J. Guo, A. Conn, *Appl. Sci.* **2019**, *9*, 2796.
[71] S. Qin, A. McTeer, *J. Appl. Phys.* **2008**, *104*, 094902.
[72] L. A. Dissado, G. Mazzanti, G. C. Montanari, *IEEE Trans. Dielectr. Electr. Insul.* **1997**, *4*, 496.
[73] R. J. Densley, R. Bartnikas, B. Bernstein, *IEEE Trans. Power Delivery* **1994**, *9*, 559.
[74] H. J. Kim, L. Paquin, C. W. Barney, S. So, B. Chen, Z. Suo, A. J. Crosby, R. C. Hayward, *Adv. Mater.* **2020**, *32*, 2000600.
[75] D. R. King, A. J. Crosby, *ACS Appl. Mater. Interfaces* **2015**, *7*, 27771.
[76] T. Hao, *Adv. Mater.* **2001**, *13*, 1847.
[77] B. D. Chin, M.-S. Chun, H. H. Winter, *Rheol. Acta* **2009**, *48*, 177.
[78] H. Conrad, Y. Li, Y. Chen, *J. Rheol.* **1995**, *39*, 1041.
[79] A. Tonazzini, A. Sadeghi, B. Mazzolai, *Soft Rob.* **2016**, *3*, 34.
[80] K. K. Mäkelä, *J. Intell. Mater. Syst. Structures* **1999**, *10*, 609.
[81] C. Cao, X. Zhao, *Appl. Phys. Lett.* **2013**, *103*, 041901.
[82] A. Sadeghi, L. Beccai, B. Mazzolai, in *2012 IEEE/RSJ Int. Conf. on Intelligent Robots and Systems (IROS)*, IEEE, Piscataway, NJ, USA **2012**, pp. 4237–4242.
[83] J. Nikitczuk, B. Weinberg, P. K. Canavan, C. Mavroidis, *IEEE/ASME Trans. Mechatronics* **2010**, *15*, 952.
[84] Y. Tian, Y. Meng, H. Mao, S. Wen, *Phys. Rev. E* **2002**, *65*, 031507.
[85] A. Zatopa, S. Walker, Y. Menguc, *Soft Rob.* **2018**, *5*, 258.
[86] C. D. Onal, D. Rus, *Bioinspir. Biomim.* **2013**, *8*, 026003.
[87] J.-W. Kim, K. Yoshida, K. Kouda, S. Yokota, *Sens. Actuators, A* **2009**, *156*, 366.
[88] B. Weinberg, J. Nikitczuk, S. Patel, B. Patritti, C. Mavroidis, P. Bonato, P. Canavan, in *2007 IEEE Int. Conf. on Robotics and Automation (ICRA)*, IEEE, Piscataway, NJ, USA **2007**, pp. 4126–4133.
[89] D. Chapuis, R. Gassert, E. Burdet, H. Bleuler, in *2008 30th Annu. Int. Conf. of the IEEE Engineering in Medicine and Biology Society*, IEEE, Piscataway, NJ, USA **2008**, pp. 3438–3442.
[90] R. Sinko, M. Karnes, J.-H. Koo, Y.-K. Kim, K.-S. Kim, *J. Intell. Mater. Syst. Struct.* **2013**, *24*, 803.
[91] J. Yang, S. S. Sun, H. Du, W. H. Li, G. Alici, H. X. Deng, *Smart Mater. Struct.* **2014**, *23*, 105023.
[92] S. Sun, H. Deng, J. Yang, W. Li, H. Du, G. Alici, M. Nakano, *Smart Mater. Struct.* **2015**, *24*, 045045.
[93] D. Leng, T. Wu, G. Liu, X. Wang, L. Sun, *J. Intell. Mater. Syst. Struct.* **2018**, *29*, 2236.
[94] Y.-H. Shih, H. Conrad, *Int. J. Mod. Phys. B* **1994**, *08*, 2835.
[95] H. J. Choi, M. S. Cho, J. W. Kim, *Korea-Aust. Rheol. J.* **2001**, *13*, 7.
[96] Z. Suo, *Acta Mech. Solida Sin.* **2010**, *23*, 549.
[97] R. E. Pelrine, R. D. Kornbluh, J. P. Joseph, *Sens. Actuators, A* **1998**, *64*, 77.
[98] S. J. A. Koh, C. Keplinger, R. Kaltseis, C.-C. Foo, R. Baumgartner, S. Bauer, Z. Suo, *J. Mech. Phys. Solids* **2017**, *105*, 81.
[99] T. Li, G. Li, Y. Liang, T. Cheng, J. Dai, X. Yang, B. Liu, Z. Zeng, Z. Huang, Y. Luo, T. Xie, W. Yang, *Sci. Adv.* **2017**, *3*, e1602045.
[100] M. Duduta, E. Hajiesmaili, H. Zhao, R. J. Wood, D. R. Clarke, *Proc. Natl. Acad. Sci. USA* **2019**, *116*, 2476.
[101] E. Acome, S. K. Mitchell, T. G. Morrissey, M. B. Emmett, C. Benjamin, M. King, M. Radakovitz, C. Keplinger, *Science* **2018**, *359*, 61.
[102] N. Kellaris, V. G. Venkata, G. M. Smith, S. K. Mitchell, C. Keplinger, *Sci. Rob.* **2018**, *3*, eaar3276.
[103] S. K. Mitchell, X. Wang, E. Acome, T. Martin, K. Ly, N. Kellaris, V. G. Venkata, C. Keplinger, *Adv. Sci.* **2019**, *6*, 1900178.
[104] C. Schunk, L. Pearson, E. Acome, T. G. Morrissey, N. Correll, C. Keplinger, M. E. Rentschler, J. S. Humbert, in *2018 IEEE/RSJ Int. Conf. on Intelligent Robots and Systems (IROS)*, IEEE, Piscataway, NJ, USA **2018**, pp. 6417–6423.
[105] W.-B. Li, W.-M. Zhang, H.-X. Zou, Z.-K. Peng, G. Meng, *Soft Rob.* **2019**, *6*, 631.
[106] A. Orita, M. R. Cutkosky, *IEEE/ASME Trans. Mechatronics* **2016**, *21*, 2836.
[107] V. Cacucciolo, J. Shintake, Y. Kuwajima, S. Maeda, D. Floreano, H. Shea, *Nature* **2019**, *572*, 516.
[108] R. D. Kornbluh, R. Pelrine, Q. Pei, R. Heydt, S. Stanford, S. Oh, J. Eckerle, in *Smart Structures and Materials 2002: Industrial and Commercial Applications of Smart Structures Technologies*, International Society For Optics And Photonics, **2002**, *4698*, pp. 254–270.
[109] R. Pelrine, R. Kornbluh, *Adv. Sci. Technol. (Durnten-Zurich, Switz.)* **2008**, *61*, 192.
[110] M. Henke, J. Sorber, G. Gerlach, *Proc. SPIE* **2012**, *8340*, 83401P.
[111] F. Carpi, G. Frediani, C. Gerboni, J. Gemignani, D. De Rossi, *Med. Eng. Phys.* **2014**, *36*, 205.

[112] W.-B. Li, W.-M. Zhang, H.-X. Zou, Z.-K. Peng, G. Meng, *Smart Mater. Struct.* **2017**, *26*, 085033.
[113] S. Dastoor, M. Cutkosky, in *2012 IEEE Int. Conf. on Robotics and Automation (ICRA)*, IEEE, Piscataway, NJ, USA **2012**, pp. 3745–3750.
[114] T. L. Sounart, T. A. Michalske, K. R. Zavadil, *J. Microelectromech. Syst.* **2005**, *14*, 125.
[115] B. Legrand, A.-S. Rollier, D. Collard, L. Buchaillot, *Appl. Phys. Lett.* **2006**, *88*, 034105.
[116] A.-S. Rollier, B. Legrand, D. Collard, L. Buchaillot, *J. Micromech. Microeng.* **2006**, *16*, 794.
[117] T. Park, K. Kim, S.-R. Oh, Y. Cha, *Soft Rob.* **2019**, *7*, 68.
[118] S. Kim, Y. Cha, *IEEE Rob. Autom. Lett.* **2020**, *5*, 3945.
[119] P.-W. Lin, C.-H. Liu, *Polymers* **2019**, *11*, 142.
[120] E. Leroy, R. Hinchet, H. Shea, *Adv. Mater.* **2020**, *32*, 2002564.
[121] M. R. Pearson, J. Seyed-Yagoobi, *IEEE Trans. Dielectr. Electr. Insul.* **2009**, *16*, 424.
[122] X. Wang, S. K. Mitchell, E. H. Rumley, P. Rothemund, C. Keplinger, *Adv. Funct. Mater.* **2020**, *30*, 1908821.
[123] R. Pelrine, R. D. Kornbluh, Q. Pei, J. Joseph, *Science* **2000**, *287*, 836.
[124] W. Yuan, L. B. Hu, Z. B. Yu, T. Lam, J. Biggs, S. M. Ha, D. J. Xi, B. Chen, M. K. Senesky, G. Grüner, Q. Pei, *Adv. Mater.* **2008**, *20*, 621.
[125] J. Zang, S. Ryu, N. Pugno, Q. Wang, Q. Tu, M. J. Buehler, X. Zhao, *Nat. Mater.* **2013**, *12*, 321.
[126] R. Pelrine, R. Kornbluh, J. Joseph, R. Heydt, Q. Pei, S. Chiba, *Mater. Sci. Eng., C* **2000**, *11*, 89.
[127] N. Bowden, S. Brittain, A. G. Evans, J. W. Hutchinson, G. M. Whitesides, *Nature* **1998**, *393*, 146.
[128] J. A. Rogers, *Science* **2013**, *341*, 968.
[129] C. Keplinger, J.-Y. Sun, C. C. Foo, P. Rothemund, G. M. Whitesides, Z. Suo, *Science* **2013**, *341*, 984.
[130] S. M. Ha, W. Yuan, Q. Pei, R. Pelrine, S. Stanford, *Adv. Mater.* **2006**, *18*, 887.
[131] X. Niu, H. Stoyanov, W. Hu, R. Leo, P. Brochu, Q. Pei, *J. Polym. Sci., Part B: Polym. Phys.* **2013**, *51*, 197.
[132] P. H. Vargantwar, A. E. Özçam, T. K. Ghosh, R. J. Spontak, *Adv. Funct. Mater.* **2012**, *22*, 2100.
[133] T. J. Wallin, J. Pikul, R. F. Shepherd, *Nat. Rev. Mater.* **2018**, *3*, 84.
[134] M. R. O'Neill, E. Acome, S. Bakarich, S. K. Mitchell, J. Timko, C. Keplinger, R. F. Shepherd, *Adv. Funct. Mater.* **2020**, *30*, 2005244.
[135] M.-P. Chang, M. M. Maharbiz, *Lab Chip* **2009**, *9*, 1274.
[136] A.-S. Rollier, M. Faucher, B. Legrand, D. Collard, L. Buchaillot, in *Dans Symposium on Design, Test, Integration and Packaging of MEMS/MOEMS - DTIP 2006*, TIMA Editions, 2007.
[137] Z. Hsain, J. H. Pikul, *Adv. Funct. Mater.* **2019**, *29*, 1905631.
[138] J. H. Pikul, J. W. Long, *MRS Bull.* **2019**, *44*, 789.
[139] J. H. Pikul, S. Özerinç, B. Liu, R. Zhang, P. V. Braun, V. S. Deshpande, W. P. King, *Sci. Rep.* **2019**, *9*, 719.
[140] Z. Yan, J. L. Hitt, J. A. Turner, T. E. Mallouk, *Proc. Natl. Acad. Sci. USA* **2020**, *117*, 12558.
[141] C. K. Chan, H. Peng, G. Liu, K. McIlwrath, X. F. Zhang, R. A. Huggins, Y. Cui, *Nat. Nanotechnol.* **2008**, *3*, 31.
[142] E. Palleau, D. Morales, M. D. Dickey, O. D. Velev, *Nat. Commun.* **2013**, *4*, 2257.
[143] B. P. Lee, S. Konst, *Adv. Mater.* **2014**, *26*, 3415.
[144] B. P. Lee, A. Narkar, R. Wilharm, *Sens. Actuators, B* **2016**, *227*, 248.
[145] B. P. Lee, M.-H. Lin, A. Narkar, S. Konst, R. Wilharm, *Sens. Actuators, B* **2015**, *206*, 456.
[146] A. B. Baker, D. F. Wass, R. S. Trask, *Smart Mater. Struct.* **2016**, *25*, 10LT02.
[147] A. B. Baker, D. F. Wass, R. S. Trask, *MRS Adv.* **2016**, *1*, 3871.
[148] A. B. Baker, D. F. Wass, R. S. Trask, in *20th Int. Conf. on Composite Materials*, ICCM, **2015**.
[149] J. H. Waite, *Int. J. Adhes. Adhes.* **1987**, *7*, 9.
[150] P. Calvo-Marzal, M. P. Delaney, J. T. Auletta, T. Pan, N. M. Perri, L. M. Weiland, D. H. Waldeck, W. W. Clark, T. Y. Meyer, *ACS Macro Lett.* **2012**, *1*, 204.
[151] R. D. Harris, J. T. Auletta, S. A. M. Motlagh, M. J. Lawless, N. M. Perri, S. Saxena, L. M. Weiland, D. H. Waldeck, W. W. Clark, T. Y. Meyer, *ACS Macro Lett.* **2013**, *2*, 1095.
[152] J. T. Auletta, G. J. LeDonne, K. C. Gronborg, C. D. Ladd, H. Liu, W. W. Clark, T. Y. Meyer, *Macromolecules* **2015**, *48*, 1736.
[153] S. Shan, S. H. Kang, J. R. Raney, P. Wang, L. Fang, F. Candido, J. A. Lewis, K. Bertoldi, *Adv. Mater.* **2015**, *27*, 4296.
[154] S.-Y. Jeon, S. H. Kang, *Nature* **2019**, *573*, 198.
[155] J. Liu, T. Gu, S. Shan, S. H. Kang, J. C. Weaver, K. Bertoldi, *Adv. Mater.* **2016**, *28*, 6619.
[156] X. Xia, A. Afshar, H. Yang, C. M. Portela, D. M. Kochmann, C. V. Di Leo, J. R. Greer, *Nature* **2019**, *573*, 205.
[157] M. T. McDowell, S. W. Lee, W. D. Nix, Y. Cui, *Adv. Mater.* **2013**, *25*, 4966.
[158] L. Baggetto, D. Danilov, P. H. L. Notten, *Adv. Mater.* **2011**, *23*, 1563.
[159] X. H. Liu, F. Fan, H. Yang, S. Zhang, J. Y. Huang, T. Zhu, *ACS Nano* **2013**, *7*, 1495.
[160] D. Morales, I. Podolsky, R. W. Mailen, T. Shay, M. D. Dickey, O. D. Velev, *Micromachines* **2016**, *7*, 98.
[161] A. B. Baker, D. F. Wass, R. S. Trask, *Sens. Actuators, B* **2018**, *254*, 519.
[162] J. Shang, X. Le, J. Zhang, T. Chen, P. Theato, *Polym. Chem.* **2019**, *10*, 1036.
[163] N. Nitta, F. Wu, J. T. Lee, G. Yushin, *Mater. Today* **2015**, *18*, 252.
[164] M. R. Zamfir, H. T. Nguyen, E. Moyen, Y. H. Lee, D. Pribat, *J. Mater. Chem. A* **2013**, *1*, 9566.
[165] A. Tutcuoglu, C. Majidi, W. Shan, *Int. J. Heat Mass Transfer* **2016**, *97*, 412.
[166] M. Biron, *Thermoplastics and Thermoplastic Composites*, William Andrew, Norwich **2018**.
[167] T. P. Chenal, J. C. Case, J. Paik, R. K. Kramer, in *2014 IEEE/RSJ Int. Conf. on Intelligent Robots and Systems*, IEEE, Piscataway, NJ, USA **2014**, pp. 2827–2831.
[168] M. C. Yuen, R. A. Bilodeau, R. K. Kramer, *IEEE Rob. Autom. Lett.* **2016**, *1*, 708.
[169] M. Taghavi, T. Helps, B. Huang, J. Rossiter, *IEEE Rob. Autom. Lett.* **2018**, *3*, 2402.
[170] A. Pourfarzaneh, M. Taghavi, T. Helps, J. Rossiter, in *2019 2nd IEEE Int. Conf. on Soft Robotics (RoboSoft)*, IEEE, Piscataway, NJ, USA **2019**, pp. 410–415.
[171] A. Firouzeh, M. Salerno, J. Paik, *IEEE Trans. Rob.* **2017**, *33*, 765.
[172] Y. Yang, Y. Chen, Y. Li, M. Zhiqiang Chen, in *2016 IEEE Int. Conf. Robot. Autom. ICRA*, IEEE, Piscataway, NJ, USA **2016**, pp. 3871–3877.
[173] Y. Yang, Y. Chen, Y. Li, M. Z. Q. Chen, Y. Wei, *Soft Rob.* **2017**, *4*, 147.
[174] B. Aksoy, H. Shea, *Adv. Funct. Mater.* **2020**, *30*, 2001597.
[175] M. A. McEvoy, N. Correll, *Science* **2015**, *347*, 1261689.
[176] M. A. McEvoy, N. Correll, *J. Compos. Mater.* **2015**, *49*, 1799.
[177] M. McEvoy, N. Correll, in *Exp. Robot.* (Eds.: M. A. Hsieh, O. Khatib, V. Kumar), Springer International Publishing, Cham, Switzerland **2016**, pp. 893–907.
[178] M. A. McEvoy, N. Correll, *Soft Rob.* **2018**, *5*, 737.
[179] A. M. Nasab, A. Sabzehzar, M. Tatari, C. Majidi, W. Shan, *Soft Rob.* **2017**, *4*, 411.
[180] M. Tatari, A. M. Nasab, K. T. Turner, W. Shan, *Adv. Mater. Interfaces* **2018**, *5*, 1800321.
[181] W. M. Huang, Z. Ding, C. C. Wang, J. Wei, Y. Zhao, H. Purnawali, *Mater. Today* **2010**, *13*, 54.
[182] C. Liu, H. Qin, P. T. Mather, *J. Mater. Chem.* **2007**, *17*, 1543.
[183] J. Eisenhaure, S. Kim, *Polymers* **2014**, *6*, 2274.
[184] J. Eisenhaure, S. Kim, *Int. J. Adhes. Adhes.* **2018**, *81*, 74.
[185] A. Tonazzini, S. Mintchev, B. Schubert, B. Mazzolai, J. Shintake, D. Floreano, *Adv. Mater.* **2016**, *28*, 10142.
[186] B. E. Schubert, D. Floreano, *RSC Adv.* **2013**, *3*, 24671.
[187] L. Zheng, S. Yoshida, Y. Morimoto, H. Onoe, S. Takeuchi, in *2015 28th IEEE Int. Conf. on Micro Electro Mechanical Systems (MEMS)*, IEEE, Piscataway, NJ, USA **2015**, pp. 18–21.
[188] W. Shan, T. Lu, C. Majidi, *Smart Mater. Struct.* **2013**, *22*, 085005.

[189] J. Shintake, B. Schubert, S. Rosset, H. Shea, D. Floreano, in *2015 IEEE/RSJ Int. Conf. on Intelligent Robots and Systems (IROS)*, IEEE, Piscataway, NJ, USA **2015**, pp. 1097–1102.
[190] S. Park, N. Baugh, H. K. Shah, D. P. Parekh, I. D. Joshipura, M. D. Dickey, *Adv. Sci.* **2019**, *6*, 1901579.
[191] K. Bhattacharya, S. Conti, G. Zanzotto, J. Zimmer, *Nature* **2004**, *428*, 55.
[192] X. Huang, M. Ford, Z. J. Patterson, M. Zarepoor, C. Pan, C. Majidi, *J. Mater. Chem. B* **2020**, *8*, 4539.
[193] E. Hawkes, B. An, N. M. Benbernou, H. Tanaka, S. Kim, E. D. Demaine, D. Rus, R. J. Wood, *Proc. Natl. Acad. Sci. USA* **2010**, *107*, 12441.
[194] J. W. Booth, D. Shah, J. C. Case, E. L. White, M. C. Yuen, O. Cyr-Choiniere, R. Kramer-Bottiglio, *Sci. Rob.* **2018**, *3*, eaat1853.
[195] X. Huang, K. Kumar, M. K. Jawed, A. M. Nasab, Z. Ye, W. Shan, C. Majidi, *Sci. Rob.* **2018**, *3*, eaau7557.
[196] M. Shahinpoor, *Proc. SPIE* **2000**, *3987*, 187.
[197] S. V. Ahir, A. R. Tajbakhsh, E. M. Terentjev, *Adv. Funct. Mater.* **2006**, *16*, 556.
[198] J. Küpfer, H. Finkelmann, *Makromol. Chem., Rapid Commun.* **1991**, *12*, 717.
[199] C. Yuan, D. J. Roach, C. K. Dunn, Q. Mu, X. Kuang, C. M. Yakacki, T. J. Wang, K. Yu, H. J. Qi, *Soft Matter* **2017**, *13*, 5558.
[200] A. Minori, S. Jadhav, Q. He, S. Cai, M. T. Tolley, in *ASME 2017 Conf. on Smart Materials, Adaptive Structures and Intelligent Systems (SMASIS)*, American Society Of Mechanical Engineers Digital Collection, **2017**.
[201] D. J. Roach, X. Kuang, C. Yuan, K. Chen, H. J. Qi, *Smart Mater. Struct.* **2018**, *27*, 125011.
[202] Y.-Y. Xiao, Z.-C. Jiang, X. Tong, Y. Zhao, *Adv. Mater.* **2019**, *31*, 1903452.
[203] Y. Y. Huang, J. Biggins, Y. Ji, E. M. Terentjev, *J. Appl. Phys.* **2010**, *107*, 083515.
[204] S. Schuhladen, F. Preller, R. Rix, S. Petsch, R. Zentel, H. Zappe, *Adv. Mater.* **2014**, *26*, 7247.
[205] Q. He, Z. Wang, Y. Wang, A. Minori, M. T. Tolley, S. Cai, *Sci. Adv.* **2019**, *5*, eaax5746.
[206] C. Wang, K. Sim, J. Chen, H. Kim, Z. Rao, Y. Li, W. Chen, J. Song, R. Verduzco, C. Yu, *Adv. Mater.* **2018**, *30*, 1706695.
[207] A. Agrawal, H. Chen, H. Kim, B. Zhu, O. Adetiba, A. Miranda, A. C. Chipara, P. M. Ajayan, J. G. Jacot, R. Verduzco, *ACS Macro Lett.* **2016**, *5*, 1386.
[208] H. Kim, J. A. Lee, C. P. Ambulo, H. B. Lee, S. H. Kim, V. V. Naik, C. S. Haines, A. E. Aliev, R. Ovalle-Robles, R. H. Baughman, T. H. Ware, *Adv. Funct. Mater.* **2019**, *29*, 1905063.
[209] J. Liu, Y. Gao, H. Wang, R. Poling-Skutvik, C. O. Osuji, S. Yang, *Adv. Intell. Syst.* **2020**, *2*, 1900163.
[210] M. J. Ford, C. P. Ambulo, T. A. Kent, E. J. Markvicka, C. Pan, J. Malen, T. H. Ware, C. Majidi, *Proc. Natl. Acad. Sci. USA* **2019**, *116*, 21438.
[211] M. J. Ford, M. Palaniswamy, C. P. Ambulo, T. H. Ware, C. Majidi, *Soft Matter* **2020**, *16*, 5878.
[212] W. Lehmann, H. Skupin, C. Tolksdorf, E. Gebhard, R. Zentel, P. Krüger, M. Lösche, F. Kremer, *Nature* **2001**, *410*, 447.
[213] Z. S. Davidson, H. Shahsavan, A. Aghakhani, Y. Guo, L. Hines, Y. Xia, S. Yang, M. Sitti, *Sci. Adv.* **2019**, *5*, eaay0855.
[214] M. A. Haq, Y. Su, D. Wang, *Mater. Sci. Eng., C* **2017**, *70*, 842.
[215] A. K. Bajpai, S. K. Shukla, S. Bhanu, S. Kankane, *Prog. Polym. Sci.* **2008**, *33*, 1088.
[216] P. Sánchez-Moreno, J. de Vicente, S. Nardecchia, J. A. Marchal, H. Boulaiz, *Nanomaterials* **2018**, *8*, 935.
[217] H. Warren, M. in het Panhuis, G. M. Spinks, D. L. Officer, *J. Polym. Sci., Part B: Polym. Phys.* **2018**, *56*, 46.
[218] X. Huang, K. Kumar, M. K. Jawed, A. Mohammadi Nasab, Z. Ye, W. Shan, C. Majidi, *Adv. Mater. Technol.* **2019**, *4*, 1800540.
[219] S. Rich, S.-H. Jang, Y.-L. Park, C. Majidi, *Adv. Mater. Technol.* **2017**, *2*, 1700179.
[220] M. T. Tolley, S. M. Felton, S. Miyashita, D. Aukes, D. Rus, R. J. Wood, *Smart Mater. Struct.* **2014**, *23*, 094006.
[221] S. M. Felton, M. T. Tolley, B. Shin, C. D. Onal, E. D. Demaine, D. Rus, R. J. Wood, *Soft Matter* **2013**, *9*, 7688.
[222] S. M. Felton, M. T. Tolley, C. D. Onal, D. Rus, R. J. Wood, in *2013 IEEE Int. Conf. on Robotics and Automation (ICRA)*, IEEE, Piscataway, NJ, USA **2013**, pp. 277–282.
[223] M. D. Bartlett, N. Kazem, M. J. Powell-Palm, X. Huang, W. Sun, J. A. Malen, C. Majidi, *Proc. Natl. Acad. Sci. USA* **2017**, *114*, 2143.
[224] H. Jin, E. Dong, M. Xu, C. Liu, G. Alici, Y. Jie, *Smart Mater. Struct.* **2016**, *25*, 085026.
[225] H. Yuan, F. Chapelle, J.-C. Fauroux, X. Balandraud, *Smart Mater. Struct.* **2018**, *27*, 055005.
[226] H.-T. Lin, G. G. Leisk, B. Trimmer, *Bioinspir. Biomim.* **2011**, *6*, 026007.
[227] H. Rodrigue, W. Wang, M.-W. Han, T. J. Y. Kim, S.-H. Ahn, *Soft Rob.* **2017**, *4*, 3.
[228] J. O. Alcaide, L. Pearson, M. E. Rentschler, in *2017 IEEE International Conference on Robotics and Automation (ICRA)*, IEEE, **2017**, pp. 4338–4345.
[229] S. Seok, C. D. Onal, K. Cho, R. J. Wood, D. Rus, S. Kim, *IEEE/ASME Trans. Mechatronics* **2013**, *18*, 1485.
[230] Y. Kim, S. S. Cheng, M. Diakite, R. P. Gullapalli, J. M. Simard, J. P. Desai, *IEEE Trans. Rob.* **2017**, *33*, 1386.
[231] Y. Wang, A. Villada, Y. Zhai, Z. Zou, Y. Chen, X. Yin, J. Xiao, *Appl. Phys. Lett.* **2019**, *114*, 193701.
[232] Y. Wang, J. Xiao, *Soft Matter* **2017**, *13*, 5317.
[233] H. Lee, D.-S. Um, Y. Lee, S. Lim, H. Kim, H. Ko, *Adv. Mater.* **2016**, *28*, 7457.
[234] J. Krahn, D. Sameoto, C. Menon, *Smart Mater. Struct.* **2011**, *20*, 015014.
[235] J. Krahn, Y. Liu, A. Sadeghi, C. Menon, *Smart Mater. Struct.* **2011**, *20*, 115021.
[236] Z. Ye, G. Z. Lum, S. Song, S. Rich, M. Sitti, *Adv. Mater.* **2016**, *28*, 5088.
[237] G. Yun, S.-Y. Tang, S. Sun, D. Yuan, Q. Zhao, L. Deng, S. Yan, H. Du, M. D. Dickey, W. Li, *Nat. Commun.* **2019**, *10*, 1300.
[238] P. A. Xu, A. K. Mishra, H. Bai, C. A. Aubin, L. Zullo, R. F. Shepherd, *Sci. Rob.* **2019**, *4*, eaaw6304.
[239] R. L. Truby, M. Wehner, A. K. Grosskopf, D. M. Vogt, S. G. M. Uzel, R. J. Wood, J. A. Lewis, *Adv. Mater.* **2018**, *30*, 1706383.
[240] J. T. Muth, D. M. Vogt, R. L. Truby, Y. Mengüç, D. B. Kolesky, R. J. Wood, J. A. Lewis, *Adv. Mater.* **2014**, *26*, 6307.
[241] A. Miriyev, K. Stack, H. Lipson, *Nat. Commun.* **2017**, *8*, 596.
[242] N. Torras, M. Duque, C. J. Camargo, J. Esteve, A. Sánchez-Ferrer, *Soft Matter* **2017**, *13*, 7264.
[243] A. B. M. T. Haque, R. Tutika, R. L. Byrum, M. D. Bartlett, *Adv. Funct. Mater.* **2020**, *30*, 2000832.
[244] R. Takahashi, T. L. Sun, Y. Saruwatari, T. Kurokawa, D. R. King, J. P. Gong, *Adv. Mater.* **2018**, *30*, 1706885.
[245] M. Woo, *Proc. Natl. Acad. Sci. USA* **2020**, *117*, 5088.
[246] Y. Lu, Q. Hu, Y. Lin, D. B. Pacardo, C. Wang, W. Sun, F. S. Ligler, M. D. Dickey, Z. Gu, *Nat. Commun.* **2015**, *6*, 10066.
[247] M. D. Bartlett, A. B. Croll, D. R. King, B. M. Paret, D. J. Irschick, A. J. Crosby, *Adv. Mater.* **2012**, *24*, 1078.
[248] H. Jin, S. Xin, C. Chuang, W. Li, H. Wang, J. Zhu, H. Xie, T. Zhang, Y. Wan, Z. Qi, W. Yan, Y.-R. Lu, T.-S. Chan, X. Wu, J. B. Goodenough, H. Ji, X. Duan, *Science* **2020**, *370*, 192.
[249] S. I. Rich, R. J. Wood, C. Majidi, *Nat. Electron.* **2018**, *1*, 102.
[250] P. Rothemund, S. Kirkman, C. Keplinger, *Proc. Natl. Acad. Sci. USA* **2020**, *117*, 16207.
[251] R. L. Truby, J. A. Lewis, *Nature* **2016**, *540*, 371.
[252] A. S. Gladman, E. A. Matsumoto, R. G. Nuzzo, L. Mahadevan, J. A. Lewis, *Nat. Mater.* **2016**, *15*, 413.

David J. Levine is a Ph.D. student in the Department of Mechanical Engineering & Applied Mechanics at the University of Pennsylvania. He received his B.S. degree in mechanical & aerospace engineering from Cornell University in 2017. His research interests include programmable stiffness technologies for soft robotics, wearable haptic devices, and virtual reality systems.

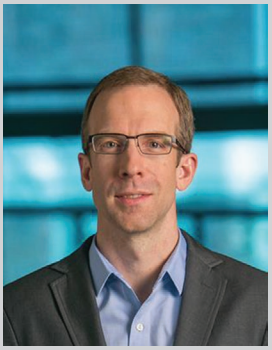

Kevin T. Turner is a Professor and the Chair of Mechanical Engineering and Applied Mechanics at the University of Pennsylvania. He holds a secondary appointment in Materials Science and Engineering. He received his B.S. from the Johns Hopkins University and S.M. and Ph.D. from the Massachusetts Institute of Technology. His research is at the nexus of mechanics, manufacturing, and materials. Ongoing research efforts in his group include structured materials with tunable adhesion and fracture properties, soft robotic grasping, design of heterogeneous and additively manufactured materials, and manufacturing of flexible hybrid electronics and sensors.

James H. Pikul is an Assistant Professor in the Department of Mechanical Engineering and Applied Mechanics at the University of Pennsylvania. He received his M.S. and Ph.D. in mechanical engineering at the University of Illinois at Urbana-Champaign where he was a Department of Energy Office of Science Graduate Research Fellow working between the fields of mechanical engineering and materials science. His research group seeks to make transformative advances in energy storage, energy conversion, multifunctional materials, and robotics by understanding and exploiting nanoscale to macroscopic characteristics of electrochemistry and soft matter.